Received: 21 November 2019 | Revised: 29 February 2020 | Accepted: 26 March 2020

DOI: 10.1096/fj.201902926R

RESEARCH ARTICLE

THE FASEB JOURNAL

Recapitulating idiopathic pulmonary fibrosis related alveolar epithelial dysfunction in a human iPSC-derived air-liquid interface model

Eva Schruf[1] | Victoria Schroeder[1] | Huy Q. Le[1] | Tanja Schönberger[2] | Dagmar Raedel[3] | Emily L. Stewart[1] | Katrin Fundel-Clemens[4] | Teresa Bluhmki[2] | Sabine Weigle[2] | Michael Schuler[2] | Matthew J. Thomas[1] | Ralf Heilker[2] | Megan J. Webster[1] | Martin Dass[3] | Manfred Frick[2] | Birgit Stierstorfer[2] | Karsten Quast[4] | James P. Garnett[1,5]

[1]Immunology & Respiratory Diseases Research, Boehringer Ingelheim Pharma GmbH & Co. KG, Biberach an der Riss, Germany

[2]Drug Discovery Sciences, Boehringer Ingelheim Pharma GmbH & Co. KG, Biberach an der Riss, Germany

[3]Nonclinical Drug Safety, Boehringer Ingelheim Pharma GmbH & Co. KG, Biberach an der Riss, Germany

[4]Global Computational Biology, Boehringer Ingelheim Pharma GmbH & Co. KG, Biberach an der Riss, Germany

[5]Institute of Cellular Medicine, Newcastle University, Newcastle upon Tyne, United Kingdom

Correspondence
James P. Garnett, Boehringer Ingelheim Pharma GmbH & Co. KG, Birkendorfer Strasse 65, 88397 Biberach an der Riss, Germany.
Email: james.garnett@boehringer-ingelheim.com

Funding information
Boehringer Ingelheim Pharma GmbH &Co.

Abstract

Idiopathic pulmonary fibrosis (IPF) is a fatal disease of unknown cause that is characterized by progressive fibrotic lung remodeling. An abnormal emergence of airway epithelial-like cells within the alveolar compartments of the lung, herein termed bronchiolization, is often observed in IPF. However, the origin of this dysfunctional distal lung epithelium remains unknown due to a lack of suitable human model systems. In this study, we established a human induced pluripotent stem cell (iPSC)-derived air-liquid interface (ALI) model of alveolar epithelial type II (ATII)-like cell differentiation that allows us to investigate alveolar epithelial progenitor cell differentiation in vitro. We treated this system with an IPF-relevant cocktail (IPF-RC) to mimic the pro-fibrotic cytokine milieu present in IPF lungs. Stimulation with IPF-RC during differentiation increases secretion of IPF biomarkers and RNA sequencing (RNA-seq) of these cultures reveals significant overlap with human IPF patient data. IPF-RC treatment further impairs ATII differentiation by driving a shift toward an airway epithelial-like expression signature, providing evidence that a pro-fibrotic cytokine environment can influence the proximo-distal differentiation pattern of human lung epithelial cells. In conclusion, we show for the first time, the establishment of a human model system that recapitulates aspects of IPF-associated bronchiolization of the lung epithelium in vitro.

Abbreviations: ALI, air-liquid interface; ATI cell, alveolar type I cell; ATII cell, alveolar type II cell; hPSC, human pluripotent stem cell; IL-13, interleukin 13; IL-1β, interleukin 1 beta; IL-33, interleukin 33; IL-4, interleukin 4; IL-8, interleukin 8; IPF, idiopathic pulmonary fibrosis; IPF-RC, IPF-relevant cocktail; iPSC, induced pluripotent stem cell; MCP1, monocyte chemotactic protein 1 (also known as CCL2); MMP, matrix metalloproteinase; RNA-seq, RNA sequencing; SAEC, small airway epithelial cell; SFTPB/C, surfactant protein B/C; TGF-β1, transforming growth factor beta 1; TNF-α, tumor necrosis factor alpha; TSLP, thymic stromal lymphopoietin.

KG; UK Medical Research Foundation Fellowship, Grant/Award Number: MRF-091-0001-RG-GARNE

KEYWORDS

alveolar epithelium, bronchiolization, induced pluripotent stem cells, IPF, pro-fibrotic milieu

1 | INTRODUCTION

Idiopathic pulmonary fibrosis (IPF) is a lethal respiratory disease characterized by progressive fibrosis of the lung parenchyma and lung function decline,[1] and despite the emergence of new therapies in nintedanib and pirfenidone that can slow down disease progression, the disease remains inevitably fatal.[2] Evidence suggests that age-related and genetic predisposition, as well as aberrant wound healing of lung epithelial micro-injuries and dysregulated fibro-proliferative repair are involved in IPF pathogenesis.[3,4] Dysfunctional epithelial repair in the IPF lung results in a loss of the normal proximo-distal patterning of the respiratory epithelium and an aberrant emergence of airway epithelial-like cell types within the alveolar regions of the lung, a phenomenon referred to as bronchiolization.[5,6] Intermediate cells types, co-expressing alveolar, and conducting airway cell selective markers, reside in these bronchiolized regions, indicative of aberrant lung epithelial differentiation.[7] Yet, the definite origin of the bronchiolized epithelial cells lining the microscopic honeycomb cysts of IPF patients remains unknown and the investigation of this complex process is complicated by a lack of suitable model systems.

The identification of specific bronchoalveolar cells as putative stem cells of the distal lung in mouse models of lung injury together with the observation of increased numbers of basal cell and club cell populations in IPF lesions have led to the hypothesis that the bronchiolized epithelium in IPF might originate from airway basal or bronchoalveolar cell migration toward alveolar regions.[8-11] However, the role of bronchoalveolar stem cells in human lung homeostasis and repair remains debatable and several recent reports strongly suggest that a specified alveolar epithelial stem cell population, constituting a subpopulation of alveolar type II (ATII) cells residing within a specific mesenchymal niche, serves as the residual stem cell pool of the alveolar epithelium.[12-16] In line with this, it has been hypothesized that the susceptibility of surfactant secreting Alveolar type II cells (ATII cells) to injury and the resulting defective alveolar repair could play a major role in IPF disease onset and progression.[15,17,18]

Limited access to primary human ATII cells, particularly from diseased patients, and the rapid loss of ATII marker expression and function when cultured in vitro, make it challenging to study the role of human ATII cells in IPF.[19] Recent advances have led to the successful derivation of ATII-like cells from human pluripotent stem cells (hPSCs, including both embryonic stem cells and induced pluripotent stem cells (iPSCs)), providing a promising alternative cell source for in vitro disease modeling.[20-26] Previous reports on hPSC-derived lung cells showed that despite their phenotypic similarities to mature lung epithelium, these models are equivalent to human fetal lung cells, rather than representing an adult state.[27,28] We propose that hPSC-derived lung epithelial cultures constitute a highly valuable model to gain insights into the role of stem cells during lung repair and regeneration due to their immature nature by which they resemble adult alveolar epithelial progenitors (AEPs), a Wnt responsive subpopulation of ATII cells recently identified as the alveolar stem cell in the human lung that shows enrichment of genes associated with lung development.[16] This is in line with previous reports, highlighting the influence of developmental pathways in lung regeneration.[29-31] Moreover, a role for aberrantly activated developmental pathways, including Wnt, SHH, Notch, and FGF signaling, has also been described in the pathogenesis of IPF, the progression of which is commonly viewed as a vicious cycle of lung injury and repair.[32-34]

In this study, we sought to investigate if iPSC-derived alveolar epithelial progenitor cells exposed to a pro-fibrotic environment could recapitulate phenotypic and functional features of the aberrant epithelial remodeling in IPF cystic lesions and thereby serve as a human in vitro model of bronchiolization. Building on previous efforts to derive alveolar epithelium from hPSCs, we first aimed to develop a novel model system that allows human ATII-like differentiation from iPSCs in 2D air-liquid interface (ALI) culture to mimic the physiological environment of the lung epithelium. We next aimed to apply this model to studying alveolar epithelial dysfunction in IPF by exposing iPSC-derived alveolar epithelial progenitor cells to an IPF-relevant cocktail (IPF-RC), based on upregulated cytokines found in IPF patient bronchoalveolar lavage or sputum.[35-43]

2 | MATERIALS AND METHODS

2.1 | Composition of an IPF-relevant cytokine cocktail (IPF-RC)

A novel IPF-RC was designed to model aspects of the IPF-related lung milieu in vitro. A panel of nine cytokines, previously reported to be upregulated in clinical IPF BAL or sputum samples compared to healthy control lungs, was selected based on a literature research. To approximately account for dilution in saline during sample collection, cytokine concentrations one order of magnitude higher than measured in IPF patient BAL were estimated as suitable for in vitro

experiments. Long-term stimulation of cells with IPF-RC was performed to simulate the cytokine milieu present in an IPF lung. The composition of IPF-RC is summarized in Table 1. All human recombinant cytokines were acquired from R&D Systems, Minneapolis, MN, US, and IPF-RC was prepared as a 1000× stock in 0.1% of BSA in PBS.

2.2 | IPF patient samples

Formalin-fixed and paraffin embedded lung samples from human IPF patients were purchased from Folio Biosciences (Powell, OH, US) under the regulatory conditions of the Boehringer Ingelheim corporate policy regarding the acquisition and use of human biospecimen. Samples were reviewed internally by a trained pathologist and the initial diagnosis of IPF was confirmed.

2.3 | Human iPSC culture

Human iPSC lines SFC065-03-03 (EBiSC: STBCi057-A, Biosamples ID: SAMEA104493762) and SFC084-03-01 (EBiSC: STBCi033-A, Biosamples ID: SAMEA104493681) were obtained from the StemBANCC consortium. iPSCs were cultured in mTeSR 1 (Stemcell Technologies, Vancouver, Canada) on hESC-qualified matrigel (Corning, New York, US) coated cell culture plates at 37°C/5% CO2 in a humidified normoxic incubator.

2.4 | Differentiation of human iPSCs into ATII-like cells in 2D ALI culture

Directed differentiation of iPSCs toward NKX2.1$^+$ lung progenitor cells was performed in serum-free differentiation medium, as previously described.[44] On day 24 of differentiation, lung progenitor cells were briefly digested with warm 0.05% of Trypsin/0.53 mM of EDTA and detached as clumps and collected via sedimentation. The cells were plated onto hESC-qualified matrigel (Corning, New York, US) coated transwell permeable support inserts (PET membrane, 12 well format, pore size 0.4 μm, Corning, New York, US) and cultured under submerged conditions until day 32 to allow the cells to attach and to spread out over the whole insert surface. Subsequently, the apical medium was removed and the cells were cultured at ALI until day 49 of differentiation. Similar to a previous study, temporal withdrawal of Wnt signaling was employed to promote distal lung epithelial progenitor differentiation toward ATII-like cells.[23] From day 24 to day 35 of differentiation, lung progenitors were cultured in SFD$^+$ medium supplemented with 3 μM CHIR99021

TABLE 1 Literature-based composition of an IPF-relevant cytokine cocktail (IPF-RC)

Cytokine	Previous investigations of IPF BAL or sputum	IPF-RC (ng/mL)
TGF-β1	32 pg/mL in IPF sputum (n = 15), undetectable in healthy sputum (n = 30)[1] 22.1 pg/mL in IPF with emphysema BAL (n = 38); 14.4 pg/mL in IPF without emphysema BAL (n = 64)[2] 1500 pg/mL in IPF BAL (n = 16)[3]	0.3
IL-1β	0.6 pg/mL in IPF BAL (n = 77), <0.3 pg/mL in healthy BAL (n = 349)[4] 2.4 pg/mL in IPF BAL (n = 11)[5]	0.01
TNF-α	1.9 pg/mL in IPF BAL (n = 11)[5] 10 pg/mL in IPF sputum (n = 15), 6.8 pg/mL in healthy sputum (n = 30)[1] 0.87 pg/mL in IPF with emphysema BAL (n = 38); 0.41 pg/mL in IPF without emphysema BAL (n = 64)[2]	0.1
IL-8	38.4 pg/mL in IPF BAL (n = 11)[5] 276 pg/mL in IPF sputum (n = 15), 46 pg/mL in healthy sputum (n = 30)[1] 35 pg/mL in IPF BAL (n = 13), 15 pg/mL in healthy BAL (n = 9)[6] 179 pg/mL in IPF with emphysema BAL (n = 38); 108 pg/mL in IPF without emphysema BAL (n = 64)[2] 44.6 pg/mL in IPF BAL (n = 7)[7]	1.5
MCP1	70 pg/mL in IPF BAL (n = 13), 5 pg/mL in healthy BAL (n = 9)[6] 555 pg/mL in IPF with emphysema BAL (n = 38); 351 pg/mL in IPF without emphysema BAL (n = 64)[2]	0.7
IL-33	4.13 pg/mL in IPF BAL (n = 100), 1.15 pg/mL in healthy BAL (n = 40)[8]	0.04
TSLP	2.5 pg/mL in IPF BAL (n = 11)[5] 9.27 pg/mL in IPF BAL (n = 100), 4.49 pg/mL in healthy BAL (n = 40)[8]	0.1
IL-13	250 pg/mL in IPF BAL (n = 16), 60 pg/mL in healthy BAL (n = 8)[9]	2.5
IL-4	16 pg/mL in IPF BAL (n = 16), 3 pg/mL in healthy BAL (n = 8)[9]	0.16

(Axon Medchem, Groningen, Netherlands), 10 ng/mL of rhKGF (R&D Systems, Minneapolis, MN, US), 10 ng/mL of rhFGF10 (R&D Systems, Minneapolis, MN, US), 25 ng/mL of dexamethasone (Sigma-Aldrich, St. Louis, MO, US), 0.1 mM of 8-Br-cAMP (Sigma-Aldrich, St. Louis, MO, US), and 0.1 mM of 3-Isobutyl-1-methylxanthine (Sigma-Aldrich, St. Louis, MO, US). Subsequently, the cells were treated with the same medium, but without CHIR99021, from day 35 to 42, before 3 μM CHIR99021 was added back for one more week until day 49 of differentiation. The culture medium was exchanged every other day during the whole maturation phase. Where indicated in the text, additional treatments were applied during differentiation from day 35 to day 49.

2.5 | Branching organoid formation of iPSC-derived lung epithelial progenitor cells

Branching of iPSC-derived lung epithelial progenitor cells was induced in 3D culture, similar to previous reports.[27] Cells were cultured in SFD^+ medium supplemented with 3 μM CHIR99021 (Axon Medchem, Groningen, Netherlands), 10 ng/mL of rhKGF (R&D Systems, Minneapolis, MN, US), and 10 ng/mL of rhFGF10 (R&D Systems, Minneapolis, MN, US). On day 24 of differentiation, lung progenitor cells were briefly digested with warm 0.05% of Trypsin/0.53 mM of EDTA and detached as clumps, which were collected at the bottom of a canonical tube via sedimentation and plated onto low attachment dishes. The following day, the resulting organoids were embedded into cold growth factor reduced matrigel (Corning, New York, US) on 48-well tissue culture plates. Following solidification of the matrigel, the organoids were covered with medium and cultured for up to 35 days. The medium was changed every 2 days.

2.6 | ATI-like differentiation of iPSC-derived ATII-like cells

ATI-like differentiation of iPSC-derived ATII cells was induced by replating cells on plastic in 2D submerged culture, as previously described.[23] On day 49 of differentiation ATII-like cells were dissociated using Gibco StemPro Accutase cell dissociation reagent (Life Technologies. Carlsbad, CA, US) and replated onto 6-well tissue culture plates in Gibco DMEM Glutamax (Life Technologies. Carlsbad, CA, US) supplemented with 10% of FBS (Life Technologies. Carlsbad, CA, US). Media was changed every other day and cells were harvested for analysis after 5 days. Controls were not replated and remained at ALI on transwell permeable support inserts until they were harvested on day 54 of differentiation.

2.7 | Primary human small airway epithelial cell culture

Primary human Small Airway Epithelial Cells (SAECs) (CC-2547, Lot 501937, Lonza, Basel, Switzerland) were thawed into a T-175 tissue culture flask and expanded for 4 days in PneumaCult-Ex Plus Medium (Stemcell Technologies, Vancouver, Canada). A single cell suspension was then created using an Animal Component-Free Cell Dissociation Kit (Stemcell Technologies, Vancouver, Canada) and 90 000 cells/cm^2 were seeded onto rat tail collagen type I (Corning, New York, US) coated transwell permeable support inserts (PET membrane, 24 well format, pore size 0.4 μm, Corning, New York, US). Four days post seeding, the apical medium was removed and the cells were differentiated at ALI in PneumaCult-ALI-S medium (Stemcell Technologies, Vancouver, Canada) for 28 days. The culture medium was exchanged every other day. Where indicated in the text, IPF-RC treatment was applied to SAEC cultures from 1 to 28 days post-ALI.

2.8 | Primary human lung fibroblast culture

Primary human lung fibroblasts (CC-2512, Lot. 0000608197, Lonza, Basel, Switzerland) were grown in fibroblast basal medium (FBM) (Lonza, Basel, Switzerland) supplemented with FGM-2 SingleQuot Kit Supplements & Growth Factors (Lonza, Basel, Switzerland) at 37°C and 5% CO_2. Cells were passaged maximum 10 times before use.

2.9 | Quantitative Real-Time PCR

RNA isolation was performed using the RNeasy Plus Mini Kit (Qiagen, Venlo, Netherlands). In some experiments, human lung total RNA (AM7968, Lot.1850512, Invitrogen, Life Technologies, Carlsbad, CA, US) was used as a positive control. Reverse transcription was performed using the Applied Biosystems High-Capacity cDNA Reverse Transcription Kit (Life Technologies, Carlsbad, CA, US). About 5 ng of cDNA were added to a final reaction volume of 10 μL containing the QuantiFast Probe PCR +ROX Vial Kit (Qiagen, Venlo, Netherlands) master mix and the respective Applied Biosystems TaqMan Gene Expression Assay FAM (Life Technologies, Carlsbad, CA, US). qPCR was performed using an Applied Biosystems ABI ViiA 7 real-time PCR System (Life Technologies, Carlsbad, CA, US). Gene expression was normalized to GAPDH control and fold change in gene expression relative to iPSCs (day 0 of differentiation) was calculated using the 2^(−ΔΔCT) method. A list of all TaqMan Gene Expression Assays used in this study is provided in Table 2.

TABLE 2 List of TaqMan Gene Expression Assays used in this study

Target	Assay ID	Vendor
ABCA3	Hs00184543_m1	Applied Biosystems
ACTA2	Hs00426835_g1	Applied Biosystems
AGER/RAGE	Hs00542584_g1	Applied Biosystems
AQP5	Hs00387048_m1	Applied Biosystems
BPIFB1	Hs00264197_m1	Applied Biosystems
CAV1	Hs00971716_m1	Applied Biosystems
CDH1	Hs01023895_m1	Applied Biosystems
COL1A1	Hs00164004_m1	Applied Biosystems
FOXA2	Hs00232764_m1	Applied Biosystems
FOXJ1	Hs00230964_m1	Applied Biosystems
GAPDH	Hs02758991_g1	Applied Biosystems
ID2	Hs04187239_m1	Applied Biosystems
KRT5	Hs00361185_m1	Applied Biosystems
MMP10	Hs00233987_m1	Applied Biosystems
MMP7	Hs01042796_m1	Applied Biosystems
MUC5AC	Hs01365616_m1	Applied Biosystems
MUC5B	Hs00861595_m1	Applied Biosystems
NKX2.1/TTF1	Hs00968940_m1	Applied Biosystems
PDPN	Hs00366766_m1	Applied Biosystems
POU5F1	Hs00999632_g1	Applied Biosystems
SCGB1A1	Hs00171092_m1	Applied Biosystems
SFTPB	Hs00167036_m1	Applied Biosystems
SFTPC	Hs00161628_m1	Applied Biosystems
SOX17	Hs00751752_s1	Applied Biosystems
SOX2	Hs01053049_s1	Applied Biosystems
SOX9	Hs00165814_m1	Applied Biosystems
TM4SF1	Hs01547334_m1	Applied Biosystems
TP63	Hs00978340_m1	Applied Biosystems

2.10 | RNA extraction, Illumina library preparation, and RNA sequencing (RNA-seq)

Total RNA of iPSC-derived day 0, day 24, and day 49 cultures (three biological replicates per timepoint) was extracted using the Ambion MagMax-96 total RNA isolation kit (Life Technologies, Carlsbad, CA, US). Nucleic acids were captured onto magnetic beads, treated with DNase, and total RNA was eluted Concentration were measured using an RNA Pico chip on a Bioanalyzer (Agilent, Santa Clara, CA, US).

A sequencing library was prepared using the TrueSeq RNA Sample Prep Kit v2-Set B (Illumina, San Diego, CA, US) with 200 ng of total RNA input per sample, resulting in an average fragment size of 275 bp including adapters. Before sequencing, eight individual libraries were normalized and pooled together using the adapter indices supplied by the manufacturer. Pooled libraries were then clustered on an Illumina cBot Instrument using the TruSeq SR Cluster Kit v3—cBot—HS (Illumina, San Diego, CA, US). Sequencing was performed as 50 bp, single reads and 7 bases index read on an Illumina HiSeq2000 instrument using the TruSeq SBS Kit HS- v3 (50-cycle) (Illumina, San Diego, CA, US).

2.11 | Bioinformatic analysis of RNA-seq data

2.11.1 | Step-by-step RNA-seq pipeline

A step-by-step bioinformatics pipeline was utilized to process and technically validate the RNA-seq data. The pipeline was described in detail in a previous study.[45]

2.11.2 | Detection of differentially expressed genes

Comparative analysis was done using the limma R-package.[46] Benjamini-Hochberg correction was used to adjust for multiple testing.

2.11.3 | Heatmaps

A heatmap of the top 500 genes deregulated in iPSC-derived day 49 cultures vs day 24 cultures was created utilizing the heatmap3 package of R statistical software and the following cutoff values: q-val < 0.001, |logFC| > 2, maxRPKM > 10.

2.11.4 | Principle component analysis (PCA)

PCA was performed as previously described, using ClustVis.[47] The top 5000 transcripts according to the coefficient of variation were selected for analysis.

2.11.5 | Gene set enrichment analysis (GSEA)

Normalized expression data for day 49 +IPF-RC and day 49 samples were analyzed using the GSEA method.[48] Genes were ranked by magnitude of correlation with a class distinction, and the GSEA algorithm determined whether members of a gene set tended to occur toward the top or bottom of the list, and calculated an enrichment score. In order to remove extremely low or not at all expressed transcripts from the data set, NGS data were filtered according to an RPKM

value > 2 in at least one of the samples. Gene sets that were significantly associated with the day 49 +IPF-RC class were identified from the C2.CP.REACTOME (Curated) collection of gene sets in the Molecular Signatures Database v6.2 (MSigDB), which comprises 674 gene sets.[49] The null distributions used to calculate the statistical significance of the enrichment scores were generated by permutation of gene sets for the day 49 +IPF-RC vs day 49 contrast (3 replicates/class). Adjustment for multiple hypothesis testing was performed by determination of FDR. Enrichment scores with an FDR q-value < 0.05 were considered to be significant.

2.11.6 | Calculation of intersections with IPF lung RNA-seq data set

Expression data for day 49 +IPF-RC and day 49 samples were compared to publicly available data for human IPF and healthy lung tissue.[50] Transcripts used for calculating the intersections were selected according to being expressed (at least one sample showing an RPKM > 2) in both data sets. This resulted in a universe of 12 365 transcripts. Deregulated transcripts were defined by exhibiting a q-value < 0.05 and an absolute log ratio of >0.5. Resulting gene sets were split into upregulated and downregulated and the intersection of the corresponding gene sets from both data sets was calculated. Significance of the intersection was tested via a hypergeometric test.

2.11.7 | ChIP Enrichment Analysis (ChEA) of RNA-seq data

Transcription factor enrichment analysis was performed on a pre-ranked gene list according to $\log_2$ fold change (adj. P-val < .05, a total of 1057 gene sets) and compared with the Literature ChIP-seq library using the web-based tool (https://amp.pharm.mssm.edu/ChEA3) available from Ma'ayan Laboratory.[51]

2.12 | Measurement of total cell number and Caspase-3/7 activity

The total cell number per insert of iPSC-derived day 49 cultures was assessed by dissociating the cultures with Gibco StemPro Accutase cell dissociation reagent (Life Technologies, Carlsbad, CA, US) and counting of cells with a TC20 Automated Cell Counter (Bio-Rad, Hercules, CA, US). Caspase-3/7 activity of day 49 cultures was measured using a Caspase-Glo 3/7 Assay Kit (Promega, Madison, WI, US).

2.13 | Measurement of MMP protein concentrations by ELISA

Matrix metalloproteinase (MMP)-7 and MMP-10 protein concentrations in cell culture supernatants were determined using a Human Total MMP-7 DuoSet ELISA (R&D Systems, Minneapolis, MN, US) and a Human Total MMP-10 DuoSet ELISA (R&D Systems, Minneapolis, MN, US).

2.14 | Flow cytometry

Flow cytometry was performed on day 24 of differentiation. Lung progenitors were dissociated and taken up into ice cold 1% of BSA in PBS. All washing steps were performed by applying ice cold wash buffer (0.1% BSA in PBS) and pelleting at 300g for 5 minutes. 1×10^6 cells were transferred into a FACS tube and washed, before prewarmed Cytofix fixation buffer (BD Biosciences, Franklin Lakes, NJ, US) was added (10 minutes at 37°C). Cells were then washed and permeabilized in 80% of MeOH for 5 minutes, followed by 0.1% of Tween-20 (Sigma-Aldrich, St. Louis, MO, US) for 10 minutes. Blocking was performed in 10% of goat serum (Sigma-Aldrich, St. Louis, MO, US) for 10 minutes. Cells were washed and incubated in the respective Alexa Fluor conjugated antibody for 30 minutes in the dark. Isotype controls were incubated in 1 µg/mL of Alexa Fluor 488 conjugated rabbit IgG Isotype Control (Abcam, Cambridge, UK) and samples for NKX2.1 staining were incubated in 1 µg/mL of Alexa Fluor conjugated anti-TTF1 antibody (Abcam, Cambridge UK). The cells were then washed, resuspended in Cellfix (BD Biosciences) and transferred through a 35 µm strainer cap. Samples were measured on a LSR II flow cytometer (BD Biosciences, Franklin Lakes, NJ, US) and analyzed using the FACSDiva (BD Biosciences, Franklin Lakes, NJ, US) and the FloJo (FlowJo LLC) software.

2.15 | Immunohistochemistry

All primary and secondary antibodies used in this study are listed in Table 3.

2.15.1 | Hematoxylin and eosin and Alcian Blue/PAS stainings

Transwell cultures were fixed for 30 minutes with 4% of Paraformaldehyde (BosterBio, Pleasanton, CA, US) at room temperature and the whole membrane was cut out of the insert for further processing. Fixed inserts were dehydrated

TABLE 3 List of antibodies used in this study

Antibody	Cat. No.	Vendor
ABCA3 (rabbit polyclonal)	ab99856	abcam
Collagen type I (mouse IgG1)	SAB4200678	Sigma-Aldrich
E-Cadherin (rabbit IgG)	3195S	Cell Signaling
FOXA2 (goat IgG)	AF2400	R&D systems
KRT5 (guinea pig polyclonal)	GP-CK5	Progen
MUC5AC (mouse IgG1k)	MA1-38223	Invitrogen
MUC5B (rabbit polyclonal)	HPA008246	Sigma-Aldrich
NKX2.1/TTF1 (mouse IgG1k)	MA5-13961	Invitrogen
NKX2.1/TTF1 (rabbit IgG)	WRAB-1231	Seven Hills
Pro-SFTPC (rabbit polyclonal)	AB3786	Millipore
SFTPB (rabbit polyclonal)	WRAB-48604	Seven Hills
SFTPC (rabbit IgG)	HPA010928	Sigma-Aldrich
SOX9 (rabbit IgG)	HPA001758	Sigma-Aldrich
Vimentin (rabbit IgG)	ab92547	abcam
KRT5 (rabbit IgG) Alexa Fluor 647 conjugated	ab193895	abcam
NKX2.1/TTF1 (rabbit IgG) Alexa Fluor 488 conjugated	ab196470	abcam
Donkey anti goat IgG Alexa Fluor 488 conjugated	A-11055	Invitrogen
Donkey anti rabbit IgG Alexa Fluor 594 conjugated	A-21207	Invitrogen
Donkey anti rat IgG Alexa Fluor 488 conjugated	A-21208	Invitrogen
Goat anti guinea pig IgG Alexa Fluor 568 conjugated	A-11075	Invitrogen
Goat anti mouse IgG Alexa Fluor 488 conjugated	A-11029	Invitrogen
Goat anti mouse IgG1 Alexa Fluor 568 conjugated	A-21124	Invitrogen
Goat anti mouse IgG Alexa Fluor 594 conjugated	A-11032	Invitrogen
Goat anti rabbit IgG Alexa Fluor 488 conjugated	A-11034	Invitrogen
Goat anti rabbit IgG Alexa Fluor 568 conjugated	A-11011	Invitrogen
Goat anti rabbit IgG Alexa Fluor 647 conjugated	A-21245	Invitrogen
Goat anti rat IgG Alexa Fluor 594 conjugated	A-11007	Invitrogen

and embedded into paraffin following standard procedures. Transwell insert cross-sections or sections of paraffin-embedded IPF lung samples of 3 μm thickness were prepared and rehydrated using a descending series of ethanol. Hematoxylin and eosin (H&E) and Alcian Blue/PAS stainings were performed according to standard protocols. Images were acquired with an AxioCam MR3 (Zeiss, Oberkochen, Germany) using the 20× objective of an Axio Imager Z1 (Zeiss, Oberkochen, Germany).

2.15.2 | Immunofluorescence of iPSC-derived and primary cells

For immunofluorescence of lung epithelial progenitor cells, VAFE cell clumps were replated and expanded on hESC-qualified matrigel (Corning, New York, US) coated glass bottom plates (12-well, No. 1.5 coverslip, 14 mm glass diameter, MatTek, Ashland, MA, US). On day 24 of differentiation, cells were fixed for 15 minutes with 4% of Paraformaldehyde (BosterBio, Pleasanton, CA, US) at room temperature. The fixed samples were washed with PBS and blocked for 1 hour at room temperature in 5% of BSA with 0.3% of TritonX-100 (Sigma-Aldrich, St. Louis, MO, US) in PBS. The cells were then incubated with the respective primary and secondary antibodies according to standard protocols. To visualize the nuclei, the cells were stained with 2 μg/mL of Hoechst 33342 (Life Technologies, Carlsbad, CA, US) for 5 minutes.

For immunofluorescence of transwell inserts, iPSC-derived ATII-like cells or primary SAEC cultures were fixed for 30 minutes with 4% of Paraformaldehyde (BosterBio, Pleasanton, CA, US) at room temperature. The inserts were then washed with PBS and the whole membrane was cut out of the insert for further processing.

Whole insert stainings were performed after blocking the fixed cells on the membrane for 1 hour at room temperature in 5% of BSA with 0.3% of TritonX-100 (Sigma-Aldrich, St. Louis, MO, US) in PBS, by incubating them in the respective primary and secondary antibodies according to standard protocols. The membranes were then washed in PBS, mounted with Invitrogen ProLong Diamond Antifade Mountant with DAPI (Life Technologies, Carlsbad, CA, US) and coverslipped.

For staining of insert cross-sections and definitive endoderm bodies, fixed specimen were dehydrated using a Tissue Tek VIP processor and embedded into paraffin blocks. Sections of 3 μm thickness were prepared, deparaffinized with xylene, and rehydrated using a descending series of ethanol. Antigen retrieval was performed for 30 minutes at 95°C in HIER sodium citrate solution (BioLegend, San Diego, CA, US). The samples were blocked for 1 hour at room temperature with 5% of normal goat or normal donkey serum (Sigma-Aldrich, St. Louis, MO, US) in PBS and incubated with the respective primary and secondary antibodies according to standard protocols. The sections were then mounted with Invitrogen ProLong Diamond Antifade Mountant with DAPI (Life Technologies, Carlsbad, CA, US) and coverslipped.

All specimens were imaged with a LSM 710 confocal microscope system (Zeiss, Oberkochen, Germany) with an

AXIO Observer Z1 using a Plan-Apochromat 20× objective or a Plan-Apochromat 40× water-immersion objective.

2.15.3 | Immunohistochemistry of IPF lung sections

Immunohistochemistry in IPF patient samples was carried out on the automated Leica IHC Bond-RX platform (Leica Biosystems, Nussloch, Germany) using the Opal method (Perkin Elmer, Waltham, MA, US). Three µm thick sections of FFPE IPF lung tissue on super frost plus slides were deparaffinized and rehydrated for multiplex immunohistochemistry staining. Antigen retrieval was performed for all primary antibodies by heating the sections in Bond ER solution 1 buffer (Leica Biosystems, Nussloch, Germany) at 95°C; pH 6.0 for 20 minutes. Primary antibodies were diluted with Leica Primary Antibody Diluent (Leica Biosystems, Nussloch, Germany) and sections were incubated with them for 30 minutes at room temperature followed by incubation (10 minutes at RT) with Opal Polymer Anti-Rabbit HRP Kit (ARR1001KT; Perkin Elmer Waltham, MA, US). Immunofluorescent signal was visualized using the OPAL (Perkin Elmer, Waltham, MA, US) TSA dye 570 and TSA dye 650 and counterstained with Spectral DAPI (Akoya, Menlo Park, CA). Microscopy of IPF lung samples was conducted with an AxioImager M2 microscope (Zeiss, Oberkochen, Germany) and images were created using an AxioScan scanner and ZEN slidescan software (Zeiss, Oberkochen, Germany).

2.16 | Semi-quantitative measurement of $SFTPC^+$ area in iPSC-derived cultures

Immunofluorescence of fixed whole transwell inserts was performed as described above. All samples of an experiment were stained and imaged on the same day. Nine randomly selected areas per insert (425.1 µm × 425.1 µm per area) were captured using a 20× Plan-Apochromat objective on a LSM 710 confocal microscope system (Zeiss, Oberkochen, Germany) with the following settings: Alexa Fluor 488 channel, 5% of laser power, master gain 600, acquisition speed 9, resolution 1024 px × 1024 px. To account for unevenness in specimen surface and thickness, Z-stack imaging of 20 vertical stacks per area was applied and maximum intensity projection was performed using the ZEN 2012 Black Edition software (Zeiss, Oberkochen, Germany). Image analysis was then performed using the Fiji for ImageJ software.[52] Each image was first converted to 8-bit format, and then, converted to binary at a threshold of 20-255. In the following, particles within areas >80 px were analyzed and summarized per image. For each analyzed transwell insert, the mean positive area per image was calculated from the nine selected areas.

2.17 | Visual collagen I quantification in primary human lung fibroblast cultures

Primary human lung fibroblasts were plated in a poly-D-lysine coated 384 CellCarrier microtiter plate from PerkinElmer in FBM with FGM-2TM Single Quots (Lonza, Basel, Switzerland) at a density of 1000 cells per well. After 24 hours, the medium was replaced by the same medium containing no serum (starvation medium). Forty-eight hours cell seeding, the starvation medium was replaced with starvation medium containing a mixture of Ficoll 70 and 400 (GE Healthcare, Chicago, IL, US; 37.5 mg/mL and 25 mg/mL, respectively), 200 µM of vitamin C, and IPF-RC (1:1000 dilution). After 72 hours, the cell culture medium was removed and cells were fixed with 100% of ice-cold methanol for 30 minutes. Next, cells were washed with PBS, permeabilized for 20 minutes using 1% of Triton-X-100 (Sigma-Aldrich, St. Louis, MO, US), washed and blocked for 30 minutes with 3% of BSA in PBS. After an additional wash step, cell nuclei were stained with 1 µM of Hoechst 33342 (Life Technologies. Carlsbad, CA, US) and collagen I was stained using a monoclonal antibody (SAB4200678, Sigma-Aldrich, St. Louis, MO, US). For primary antibody detection, cells were washed and incubated for 30 minutes at 37°C with Goat anti mouse IgG1 Alexa Fluor 568 secondary antibody. After secondary antibody removal, cells were stained with Invitrogen HCS Cell Mask Green stain (1:50 000, Life Technologies. Carlsbad, CA, US). Following a final wash step, images were acquired in an InCell 2200 Analyzer (GE Healthcare, Chicago, IL, US), using 2D-Deconvolution for nuclei (Hoechst channel), cells (FITC channel), and collagen I (TexasRed channel), and images were transferred to the Columbus Image Storage and Analysis system (Perkin Elmer, Waltham, MA, US).

Image analysis was performed as previously described.[53,54] Briefly, using the building blocks of Perkin Elmer´s Columbus Image Analysis system, first nuclei acquired with the Hoechst channel were detected using the building block (BB) "nuclei." Second, cells were defined with the BB "find cytoplasm" from the FITC channel. Collagen I area was defined by two individual BBs "find simple image region" based on images acquired in the TexasRed channel. Collagen I readouts were normalized to the number of cells per image field. Total number of cells, and total collagen area/total number of cells were used as parameters to quantify effects of IPF-RC.

2.18 | Transmission electron microscopy

For electron microscopy of iPSC-derived ATII-like cells, transwell inserts were prefixed for 1 hour with 4% of

Paraformaldehyde. The PET membrane with prefixed cells was then washed with a 0,1% of cacodylate buffer solution for 30 minutes. Afterward, the samples were transferred into an EM-TP Tissue processor (Leica Microsystems, Wetzlar, Germany) for automated postfixation, staining, dehydration, and embedding. In detail, the samples underwent the following steps: 20 minutes in 0,1% of cacodylate buffer, 3 hours in 1% of Daltons osmium tetroxide aq., three times 15 minutes in 0,1% of cacodylate buffer solution, 15 minutes in 30% of isopropanol, 30 minutes each in 30%, 50%, 70%, 90%, and 100% isopropanol, and three times 1 hour in 100% of isopropanol. Following dehydration, sample infiltration with Epoxy resin was achieved as follows: 30 minutes in 50% of isopropanol/50% EPON, 30 minutes in 33% of isopropanol/66% EPON, 30 minutes in 20% of isopropanol/80% EPON, and 60 minutes in 100% of EPON. The samples were then incubated twice for 6 hours in 100% of EPON and hardened at 60°C for 24 hours. Ultrathin sections (50 nm) were prepared on an Ultracut UCT ultra-microtome (Leica Microsystems, Wetzlar, Germany) and imaged on a TEM 912AB (Zeiss, Oberkochen, Germany).

2.19 | LysoTracker Green DND-26 live cell staining

iPSC-derived ATII-like cells were replated onto Nunc 8-well Lab-Tek Chambered Coverglasses (Thermo Fisher Scientific, Waltham, MA, US) and were allowed to attach overnight, before 100 nM LysoTracker Green DND-26 (Invitrogen, Life Technologies, Carlsbad, CA, US) was added into the medium and the cells were incubated for 20 minutes at 37°C protected from light. The medium was then removed and the samples were washed once with prewarmed Gibco FluoroBrite DMEM (Life Technologies, Carlsbad, CA, US), followed by a 5 minutes incubation in 5 ng/mL of Hoechst 33342 (Life Technologies, Carlsbad, CA, US) in FluoroBrite. Subsequent to three additional washes with FluoroBrite DMEM, fresh FluoroBrite DMEM was added to the cells and the samples were immediately imaged using a Plan-Apochromat 63× oil-immersion objective on an LSM 710 confocal microscope system (Zeiss, Oberkochen, Germany).

2.20 | Cilia beat measurements in primary small airway cultures

Cilia beat frequency was calculated from image stacks of 2D+time. Six evenly distributed regions of a transwell insert were imaged using the 32× objective of an Axiovert 25 microscope (Zeiss, Oberkochen, Germany) and an acA 1300-200 µm black and white USB-3.0 high speed camera (Basler, Ahrensburg, Germany). Ciliary movement was recorded at 100 frames per second for a total of 6 seconds per region. Applications for image capture and analysis were developed using the HALCON 13.0.2 machine vision software toolbox (MVTec Software, Munich, Germany). Visualization of image stack was performed with Analyze (AnalyzeDirect, Overland Park, KS, US). A grey value time course was calculated for each pixel over 512 frames per region. The area covered by motile cilia was determined by quantifying the percentage of pixels with a measurable beating frequency within a region. The mean ciliary beating frequency of a region was determined by calculating the average frequency of the change in grey values.

2.21 | Transepithelial electrical resistance (TEER) measurements

Transwell cultures were washed with pre-warmed PBS, before transepithelial electrical resistance (TEER) was measured using a STX-2 chopstick electrode attached to an EVOM^2 Epithelial Volt/Ohm Meter (World Precision Instruments, Sarasota, FL, USA). The raw values were multiplied with the area of the transwell insert membrane to obtain the final TEER values in $\Omega*cm^2$.

2.22 | FITC-Dextran permeability assay

For dextran flux measurements in day 28 SAEC ALI cultures, the medium in the basolateral compartment of the transwell cultures was substituted with RPMI w/o phenol red (Gibco, Waltham, MA, USA). About 5 mg/mL of 10 kDa FITC-Dextran (Sigma-Aldrich, St. Louis, MO) in RPMI w/o phenol red was then added to the apical compartment of the insert and the cells were incubated at 37°C 5% CO_2. About 10 µL-samples were taken from the basolateral compartment after 0, 30, 60, and 90 minutes and the relative fluorescence intensity (excitation 490 nm, emission 520 nm) was measured using a SpectraMax M5 (Molecular Devices, San Jose, CA, USA).

2.23 | Primary human small airway basal cell proliferation assay

Primary human small airway basal cells (Lonza, Basel, Switzerland) were thawed and expanded for 4 days in PneumaCult-Ex Plus Medium (Stemcell Technologies, Vancouver, Canada), before 3×10^3 cells/well were seeded onto 96-well tissue culture plates. Twenty-four hours after seeding, the cells were stimulated with IPF-RC or 0.0001% of BSA in PneumaCult-Ex Plus Medium. Cell proliferation was determined after 0, 24, 48, and 72 hours using the

CyQUANT Direct Cell Proliferation Assay Kit (Invitrogen, Life Technologies, Carlsbad, CA, US) according to the manufacturer's instructions.

2.24 | Statistical analysis

All qRT-PCR, ELISA, flow cytometry, and image analysis data are presented as mean with error bars representing the SD of at least three independent experiments. Experiments comparing two conditions only were analyzed using two-tailed unpaired Student's *t* test, when variances were homogeneously distributed, or Mann-Whitney U-test, when data were not normally distributed. Experiments containing three or more conditions were assessed by two-way ANOVA, followed by the Tukey test. Data analysis was performed using GraphPad Prism 8.0 (GraphPad Software). Significance values are marked as $*P < .05$, $**P < .01$, $***P < .001$ and $****P < .0001$.

3 | RESULTS

3.1 | Differentiation of human iPSCs toward ATII-like cells in ALI culture

We established a directed step-wise differentiation protocol to derive ATII-like cells from human iPSCs, in which distal lung progenitor maturation toward ATII-like cells was carried out on transwell inserts at ALI to mimic the physiological environment of the mature alveolar epithelium (Figure 1A). Adapting a previously published protocol,[20,44] we generated NKX2.1$^+$/FOXA2$^+$/SOX9$^+$ lung epithelial progenitor cells, via SOX17$^+$ definitive endoderm and ventralized anterior foregut endoderm (Figures 1B-D and S1A,B). 3D matrigel culture was utilized to confirm the budding and branching potential of the iPSC-derived lung epithelial progenitor cells, which constitutes a key functional feature of fetal epithelial progenitors during lung morphogenesis (Figure S1C). Subsequently, to induce ATII-like differentiation, day 24 lung epithelial progenitor cells were seeded onto transwell inserts and confluent cultures were further differentiated at air-liquid-interface until day 49, with temporal modulation of Wnt signaling applied to drive further differentiation of NKX2.1$^+$ lung progenitor cells toward ATII-like cells.[23] *SFTPC*, Surfactant Protein B (*SFTPB),* and *ABCA3* expression was induced over time (Figure 1E), together with an upregulation of many other ATII associated transcripts by day 49 (Figure 1F). Cells differentiated at air-liquid-interface displayed upregulated expression levels of *SFTPC*, *SFTPB,* and *ABCA3* compared to submerged conditions, while no induction of the ATI markers *CAV1* or *PDPN* was observed under either condition (Figure 2A). Immunofluorescence showed the homogeneous expression of the pan-epithelial marker E-Cadherin and confirmed the presence of SFTPC$^+$, SFTPB$^+$, and ABCA3$^+$ cells, indicative of an ATII cell phenotype (Figure 2B). Day 49 cultures also showed upregulated expression of the human alveolar epithelial progenitor marker *TM4SF1* compared to iPSCs. Moreover, a moderate induction of basal cell markers (*KRT5*, *TP63*) and other airway related transcripts (*SCGB1A1*, *MUC5B*, and *FOXJ1*) was observed and rare individual KRT5$^+$ cells could be detected, indicating that in addition to ATII-like cells, our model system contains airway basal-like cells (Figure S2A,B). Staining of cross-sectioned day 49 transwell cultures revealed that SFTPC$^+$ cells resided mainly on the apical air-exposed surface of the cultures (Figure 2C). ATII-specific lamellar body-like structures were observed (Figure 2D) and live-stained iPSC-derived ATII-like cells contained large organelles displaying intensive accumulation of LysoTracker Green DND-26 (Figure 2E). Single cell dissociation and replating of iPSC-derived ATII-like cells under 2D submerged conditions in serum-containing medium resulted in downregulated *SFTPC*, *SFTPB*, and *ABCA3* expression and upregulated expression of the ATI markers *CAV1* and *PDPN*, consistent with ATI-like differentiation potential (Figure S2C). No vimentin$^+$ cells were detected in day 49 cultures by immunofluorescence, suggesting that mesenchymal cells were absent in the iPSC-derived ALI model (Figure S2D). Our ATII differentiation protocol was reproducible in an alternative human iPSC line (Figure S3).

3.2 | iPSC-derived distal lung epithelial progenitor differentiation in the presence of an IPF-relevant cytokine cocktail (IPF-RC) results in IPF-related changes in expression signature and secretory state

We utilized our iPSC-derived model system to investigate the effects of a pro-fibrotic environment on ATII cell differentiation. An IPF-relevant cytokine cocktail (IPF-RC) was designed and was capable of inducing collagen I formation in primary human lung fibroblasts (Figure S4). The IPF-RC, contains nine cytokines previously shown to be upregulated in IPF bronchoalveolar lavage or sputum samples compared to healthy controls (Transforming growth factor beta 1 (TGF-β1), Interleukin 1 beta (IL-1β), Tumor necrosis factor alpha (TNF-α), Interleukin 8 (IL-8), Monocyte chemotactic protein 1 (MCP1), Interleukin 33 (IL-33), Thymic stromal lymphopoietin (TSLP), Interleukin 13 (IL-13), and Interleukin 4 (IL-4); Table 1). IPF-RC was applied to iPSC-derived alveolar epithelial progenitor cells for 2 weeks, following the induction of *SFTPC* expression (Figures 1E and 3A). No changes in total cell number or caspase-3/7 activity were detected upon IPF-RC treatment, indicating that

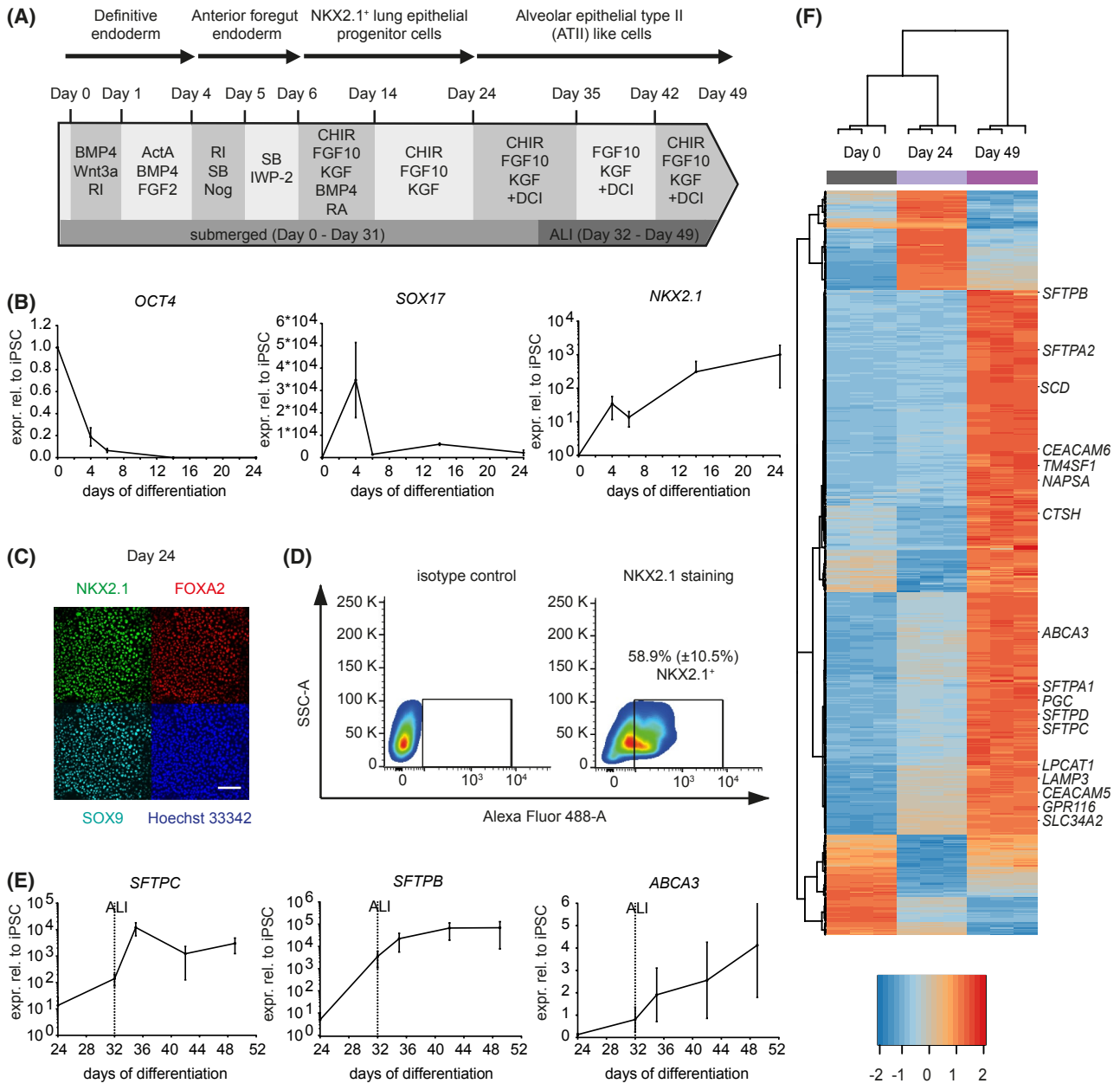

FIGURE 1 Transcriptional changes characteristic of distal lung development induced during directed differentiation of human iPSCs. A, iPSC (line SFC065-03-03) to ATII-like cell differentiation protocol. RI = Y-27632; ActA = Activin A; SB = SB431542; Nog = Noggin; RA = all-trans retinoic acid; CHIR = CHIR99021; DCI = dexamethasone, 8-Br-cAMP, IBMX. B, Transcription factor gene expression from day 0 to day 24 of differentiation normalized to GAPDH relative to day 0. Mean fold change ±SD. N = 3. C, Immunofluorescence of day 24 lung progenitors stained against NKX2.1, FOXA2, and SOX9. Nuclei stained with Hoechst 33342. Scale bar 50 µm. D, Flow cytometry analysis of NKX2.1$^+$ cells on day 24. Mean percentage of NKX2.1$^+$ cells (±SD) is indicated. N = 3. E, ATII marker gene expression from day 24 to day 49 of differentiation normalized to GAPDH relative to day 0. ALI = start of air-liquid interface. Mean fold change ±SD. N = 3. F, Heatmap of top deregulated genes in day 49 vs day 24 cultures by RNA-seq (cutoff: q-val < 0.001, |logFC|> 2, maxRPKM > 10) with known ATII marker genes labelled on the right. Day 0 = iPSCs. Day 24 = lung epithelial progenitors. Day 49 = ATII-like cells

IPF-RC did not exert any anti-proliferative or pro-apoptotic effects (Figure 3B,C). qRT-PCR revealed an upregulated expression of the IPF-related marker genes *MMP7*, *MMP10*, and *BPIFB1* and significantly increased MMP-7 and MMP-10 protein levels were detected in the culture medium of day 49 cultures stimulated with IPF-RC by ELISA, while the expression of *CDH1*, *ACTA2*, and *COL1A1* was not altered (Figures 3D and S5).

RNA-seq was performed to further investigate IPF-RC mediated transcriptional changes (Figure 3E). In accordance with an upregulation of MMP-7 and MMP-10 secretion, gene set enrichment analysis revealed a significant enrichment of

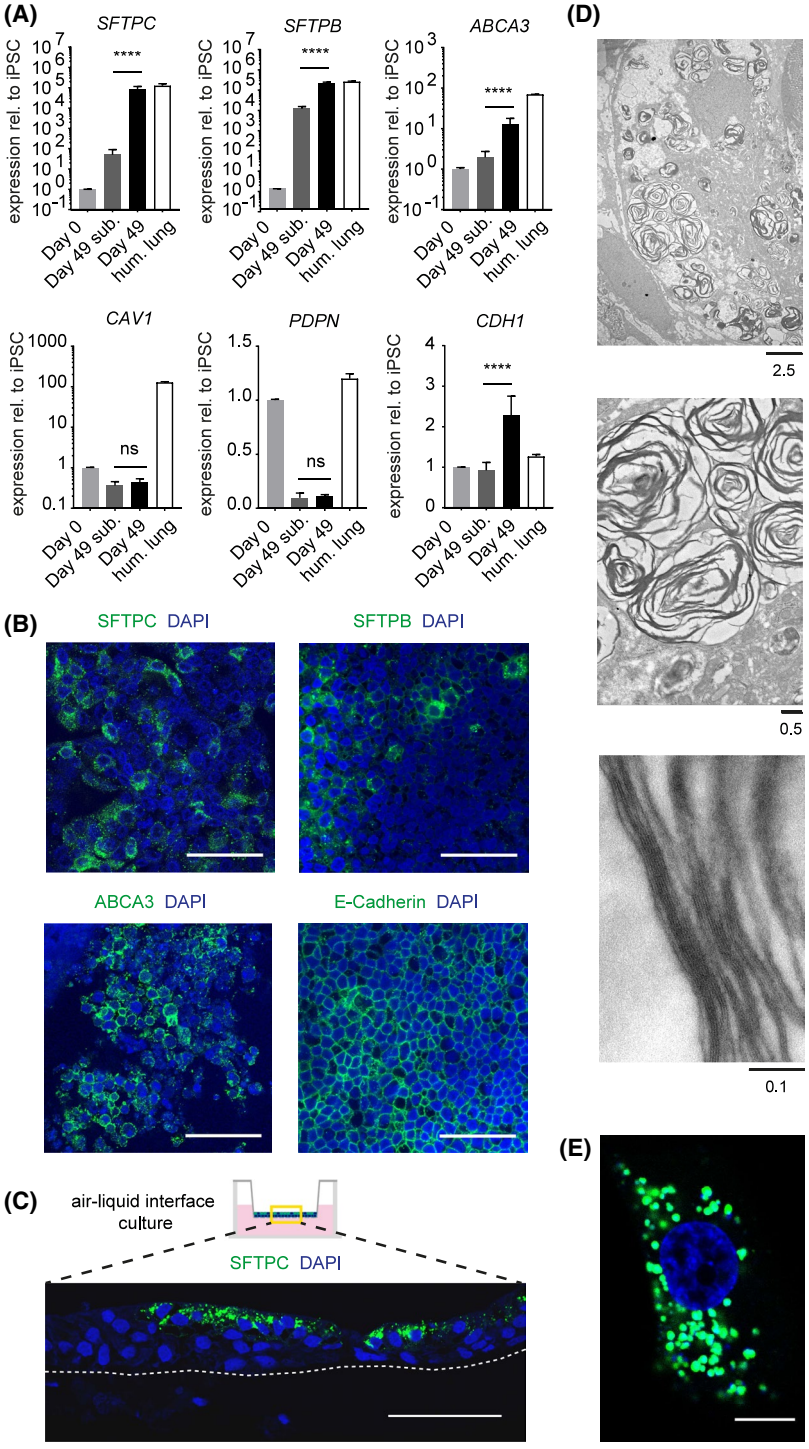

FIGURE 2 ATII-like phenotype of iPSC-derived air-liquid interface (ALI) cultures. A, Alveolar epithelial marker gene expression on day 49 of differentiation normalized to GAPDH relative to day 0. Day 49 sub. = submerged conditions. Day 49 = ALI from day 32 of differentiation onward. Hum. lung = total human lung control. Mean fold change ±SD. N = 3. ns not significant, ****$P < .0001$ by Mann-Whitney U-test. B, Immunofluorescence of day 49 cultures stained against SFTPC, SFTPB, ABCA3, or E-Cadherin. Nuclei stained with DAPI. Scale bars 50 µm. C, Immunofluorescence of a day 49 ALI culture cross-section stained against SFTPC. Nuclei stained with DAPI. Dashed line indicates PET membrane of transwell insert. Scale bar 50 µm. D, Lamellar body-like structures in day 49 cultures identified by transmission electron microscopy. Scale bars in µm. E, LysoTracker Green live-staining of iPSC-derived ATII-like cell. Nucleus stained with Hoechst 33342. Scale bar 10 µm

transcripts associated with extracellular matrix organization (among top 10 associated gene sets under investigation; C2.CP. REACTOME (Curated)) for the day 49 +IPF-RC phenotype (Figure 3F). We also compared the expression data from our iPSC-derived model to a publicly available data set for human IPF and healthy lung tissue.[50] Calculation of the intersection of these data sets revealed a significant overlap of both downregulated ($P = 4.32 \times 10^{-16}$) and upregulated ($P = 2.5 \times 10^{-29}$) transcripts between day 49 cultures treated with IPF-RC and human IPF lungs (Figure 3G). Epithelial cell adhesion related transcripts (*GJB1*, *TJP2*, *PCDH1*, and *OCLN*), as well as transcripts that are known to be repressed in IPF, including *KLF4*, *VEGFA*, *IL32*, and *SLC19A3*, were among the downregulated genes, while *MMP10* and the airway epithelial associated transcripts *BPIFB1*, *SOX2*, *PAX9*, *TP63*, *FOXJ1*, *SCGB1A1*, and *KRT5*, were upregulated in both data sets. ChIP Enrichment Analysis (ChEA) of deregulated genes was performed to investigate, which transcription factors could be potential upstream

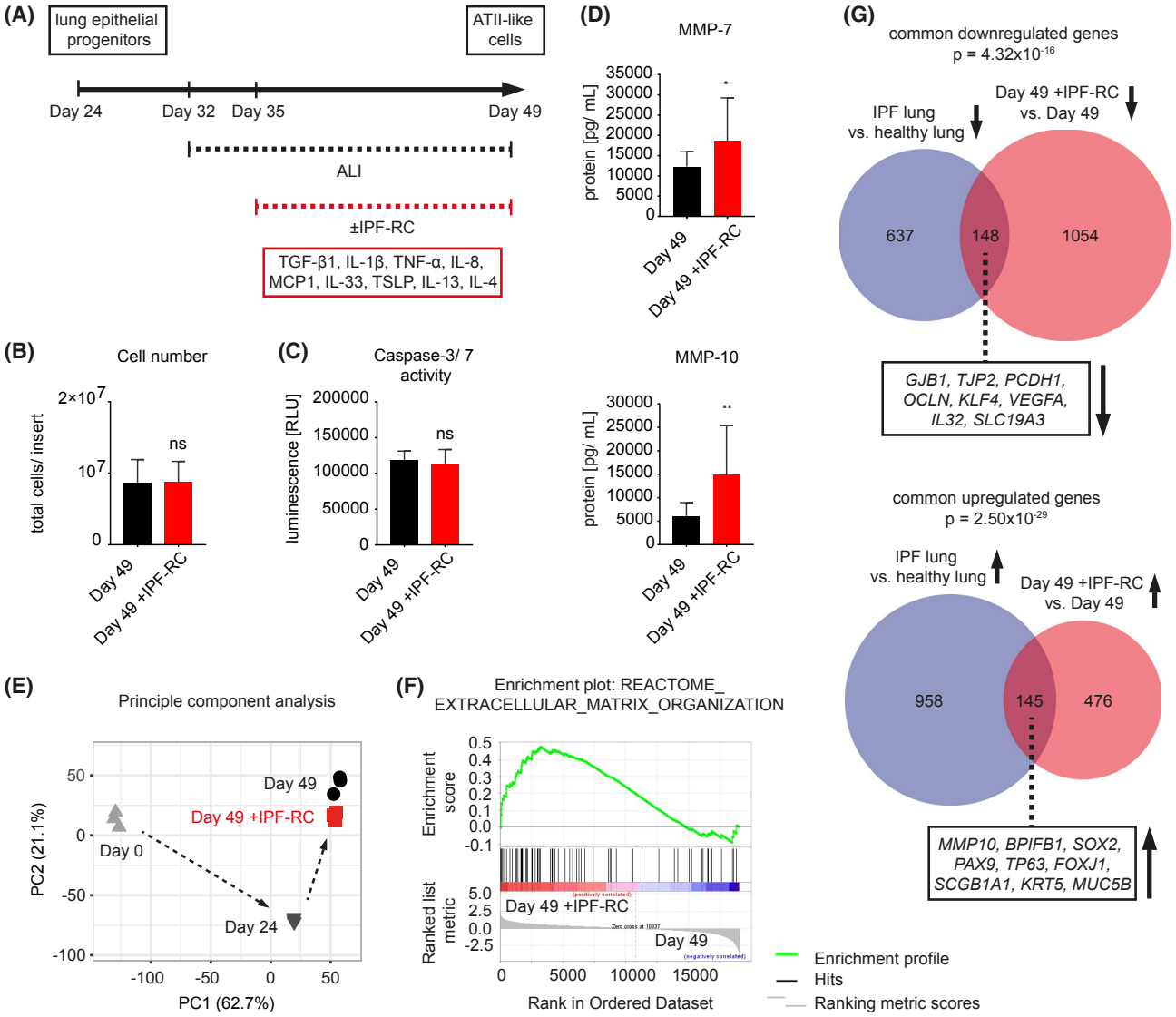

FIGURE 3 Fibrosis-related changes in transcriptional and secretory state caused by differentiation of iPSC-derived lung epithelial progenitors in the presence of an IPF-relevant cytokine cocktail (IPF-RC). A, IPF-RC stimulation during alveolar epithelial differentiation (day 35-day 49). B, Total cell number per transwell insert. Day 49 = iPSC-derived ATII-like cells (control). Day 49 +IPF-RC = iPSC-derived cells treated with IPF-RC from day 35 of differentiation onward. Mean ± SD. N = 4. ns not significant by Mann-Whitney U-test. C, Caspase-3/7 activity. Mean ± SD. N = 3. ns not significant by Mann-Whitney U-test. D, MMP-7 and MMP-10 protein levels in culture medium measured by ELISA. Mean ± SD. N = 3. $*P < .05$, $**P < .01$ by Mann-Whitney U-test. E, Principal component analysis of RNA-seq data representing the top 5000 transcripts according to the coefficient of variation. Arrows represent experimental timecourse. F, Enrichment plot for the extracellular matrix organization gene set from Reactome. FDR q-value = 0.039. G, Intersection between deregulated transcripts in IPF-RC treated iPSC-derived day 49 cultures (vs untreated) and deregulated transcripts in human IPF lung tissue (vs healthy). Cutoff: q-val < 0.05, |logFC| > 0.5, maxRPKM > 2. Top section represents downregulated, bottom section upregulated transcripts. Boxes contain examples of commonly upregulated or downregulated transcripts

drivers of the transcriptomic changes in IPF-RC treated iPSC-derived day 49 cultures (Figure S6). Interestingly, SOX2, a transcription factor known to be expressed in atypically differentiated epithelial cells of bronchiolized regions in IPF lungs, was identified as a putative regulator of the transcriptomic signature associated with IPF-RC treatment. These results indicate that IPF-RC stimulation of our iPSC-derived ALI model system allows for the recapitulation of IPF-relevant processes and transcriptional changes, in vitro.

3.3 | IPF-RC stimulation induces a shift in iPSC-derived distal lung epithelial progenitor cell differentiation toward a proximalized phenotype

As RNA-seq revealed that known airway epithelial related transcripts were among the upregulated transcripts upon IPF-RC stimulation, we sought to determine if treatment with IPF-RC had the potential to alter the proximo-distal

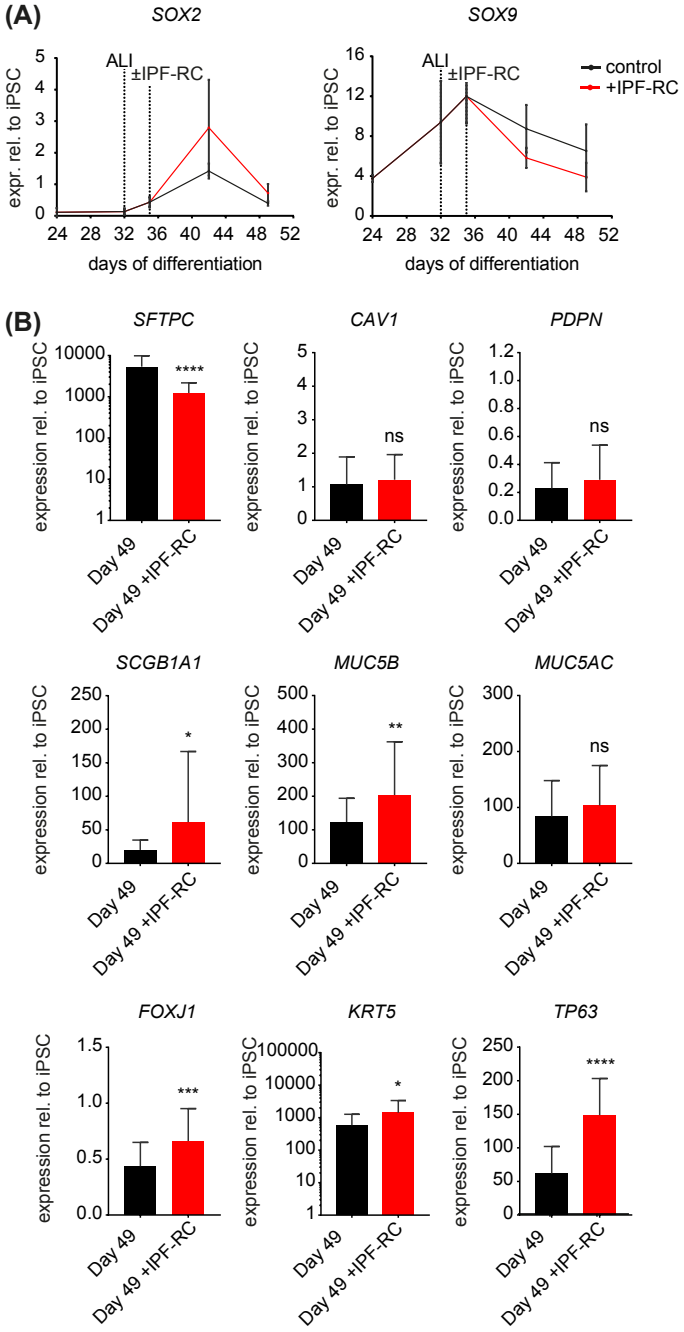

FIGURE 4 IPF-RC-induced distal-to-proximal shift in gene expression of iPSC-derived lung epithelial cultures. A, SOX2 and SOX9 expression from day 24 to day 49 of differentiation normalized to GAPDH relative to day 0. ALI = start of air-liquid interface. ±IPF-RC = start of IPF-RC/vehicle treatment. Mean fold change ±SD. N = 3. B, Alveolar and airway epithelial marker expression in day 49 cultures ±IPF-RC treatment normalized to GAPDH relative to day 0. Mean fold change ±SD. N = 9. ns not significant, *$P < .05$, **$P < .01$, ***$P < .001$ and ****$P < .0001$ by two-tailed Student's *t* test

differentiation pattern of iPSC-derived lung epithelial progenitors. Elevated expression of the transcription factor *SOX2* and reduced expression of *SOX9* were observed upon IPF-RC stimulation, both of which are central players in proximo-distal epithelial patterning during lung development (Figure 4A). IPF-RC treated cultures displayed significantly reduced expression of ATII-specific *SFTPC*, while the airway related transcripts *SCGB1A1*, *MUC5B*, *FOXJ1*, *KRT5*, and *TP63*, which are also expressed in the abnormal epithelium lining cystic lesions found in distal IPF lungs, were significantly upregulated (Figure 4B). *MUC5AC* remained unchanged upon IPF-RC treatment, indicating that goblet cell associated mucin induction was specific to MUC5B, similar to the bronchiolized epithelium in IPF patients. Expression of *CAV1* and *PDPN* was not altered, indicating that differentiation of ATII-like cells toward ATI-like cells did not contribute to the loss of *SFTPC* expression.

To understand the relative contribution of mediators within the IPF-RC, individual components were removed from the cocktail. We focused in particular on the influence of IL-13, TGF-β1, and TNF-α due to their known ability to induce epithelial remodeling. Day 49 cultures differentiated in the presence of IPF-RC without IL-13 expressed higher levels of *SFTPC* than cells treated with the full cytokine cocktail, and

displayed lower expression of *MMP10*, *BPIFB1*, *MUC5B*, *FOXJ1*, and *TP63*, suggesting IL-13 as the predominant driver of the IPF-related effects exerted by IPF-RC (Figure S7A). However, removal of IL-13 did not reduce the expression of *MMP7*, *SCGB1A1*, and *KRT5* compared to the full cocktail. Furthermore, stimulation with 2.5 ng/mL of IL-13 alone resulted in a significant downregulation of *SFTPC* expression and upregulation of *FOXJ1* and *TP63* expression, but did not alter the expression of *MMP10*, *BPIFB1*, or *MUC5B*, indicating that IL-13 was not solely responsible for the proximalization effect of IPF-RC (Figure S7B). IPF-RC without TGF-β1 led to a reduction in MUC5B expression compared to the full cocktail, yet failed to reduce IPF-RC mediated expressional changes in any of the other transcripts analyzed (Figure S7A). Removal of TNF-α did not result in a reduced induction of any IPF- or airway-associated transcripts compared to IPF-RC (Figure S7A). Moreover, TGF-β1 or TNF-α removal failed to rescue *SFTPC* expression. These results indicate that TGF-β1 and TNF-α were not the main drivers of the bronchiolization-like effect cause by IPF-RC in our model system. The individual removal of the other six cytokines (IL-1β, IL-8, MCP1, IL-33, TSLP, and IL-4) from the IPF-RC did not induce any significant alterations in the expression of IPF-related transcripts (*MMP10, BPIFB1*), of airway related transcripts, including *MUC5B* and *TP63,* nor of ATII-specific *SFTPC* compared to the full cocktail (Figure S8). These findings suggest that no individual cytokine was the sole driver of the effect of IPF-RC on iPSC-derived epithelial cultures.

Nintedanib, a tyrosine kinase inhibitor known to slow down IPF-related lung function decline, only showed some minor effects on *SCGB1A1* and *TP63* expression at clinically relevant concentrations (100 nM), but was neither able to rescue induction of IPF- and other airway-related marker genes, nor the reduction in *SFTPC* expression in IPF-RC treated cells (Figure S9).

In accordance with the reduced *SFTPC* expression in IPF-RC cultures, the mean surface area covered by $SFTPC^+$ cells was significantly reduced in day 49 IPF-RC cultures compared to controls, indicating a loss of ATII-like cells (Figure 5A,B). Histological analysis of cross-sectioned day 49 cultures revealed that IPF-RC stimulation resulted in the emergence of Alcian Blue/PAS^+ cell clusters, displaying a secretory cell-like morphology (Figure 5C). Moreover, areas of $MUC5B^+$ goblet-like cells, which were absent in controls, were detected in IPF-RC cultures by immunofluorescence (Figure 5D). These results show that IPF-RC led to the emergence of $MUC5B^+$ secretory cells, which are also frequently observed lining cystic lesions in the distal lung of IPF patients, at the expense of ATII-like cell differentiation.

3.4 | IPF-RC treatment during primary small airway basal cell differentiation favors $MUC5AC^+$ goblet cell and impairs ciliary cell formation

As airway basal cells have been proposed as a source of the bronchiolized distal lung epithelium in IPF, we also assessed the effect of IPF-RC treatment on primary small airway basal cell differentiation at ALI. Similar to our iPSC-derived cultures, IPF-RC stimulation-induced upregulated expression of *KRT5*, *TP63*, *MMP7*, *MMP10*, and *BPIFB1*, as well as increased secretion of MMP-7 and MMP-10 in small SAEC cultures (Figure 6A-C). Conversely, expression of *SCGB1A1* and *FOXJ1* decreased compared to control cultures and *MUC5AC* expression was enhanced, while no significant deregulation of *MUC5B* expression could be detected, the upregulation of which has been linked to epithelial dysfunction in IPF. TEER and dextran permeability measurements revealed that IPF-RC treatment resulted in a reduction of epithelial barrier integrity in SAEC ALI cultures (Figure S10). Cilia formation and ciliary function were also severely impaired in IPF-RC treated small airway epithelium (Figure 6D). These results indicate that the effect of IPF-RC on primary small airway basal cell differentiation differs from its effect on iPSC-derived alveolar epithelial progenitor cell differentiation.

We further examined the effect of IPF-RC stimulation on primary human small airway basal cell proliferation in submerged culture (Figure S11). No significant difference was detected between treated cultures and vehicle controls, suggesting that IPF-RC does not induce a proliferative expansion of airway basal cells.

3.5 | The metaplastic epithelium lining cystic lesions in IPF lungs contains atypical transition zones between $SFTPC^+$ ATII-like cells and $MUC5B^+$ goblet-like cells

To confirm the relevance of the findings observed in our model system for human disease, immunofluorescence in IPF patient lung sections was performed. The heterogeneous cystic lesions found in the dense fibrotic tissue of the distal IPF lungs were lined by a simple single-layered columnar or cuboidal epithelium, interrupted by areas of epithelial denudation and areas of multi-layered hyperplastic epithelium. Double immunofluorescence against SFTPC and MUC5B was performed in three IPF lungs. In accordance with previous reports that identified $MUC5B^+$ secretory cells as the predominant mucus cell type in the honeycomb epithelium, many of the cystic lesions found in the distal

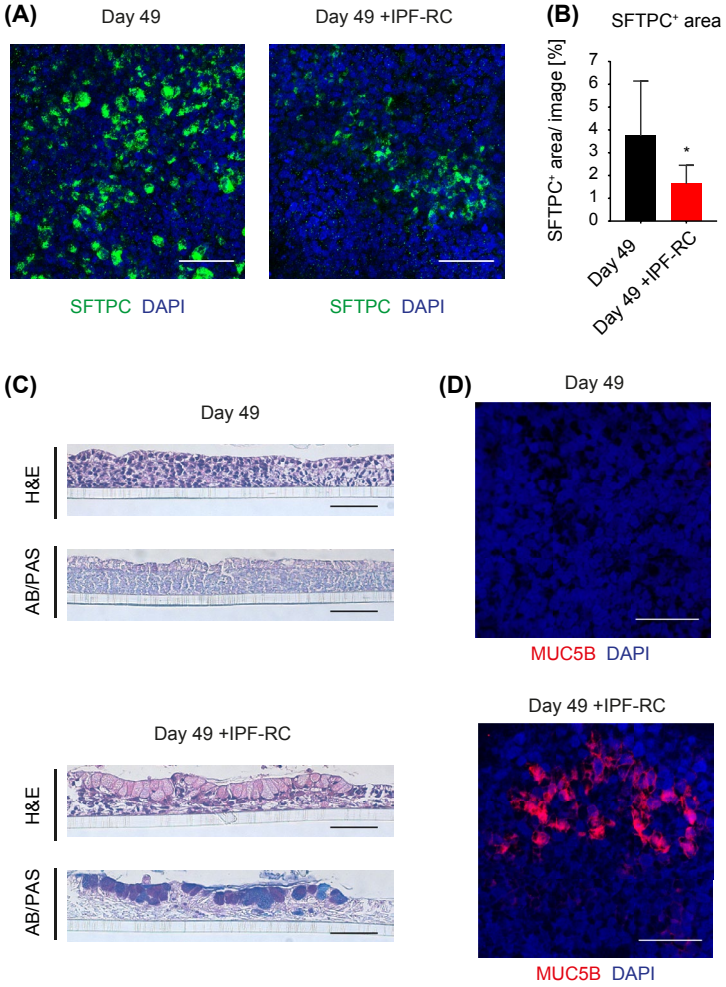

FIGURE 5 Epithelial phenotypic changes recapitulating aspects of IPF-related bronchiolization resulting from IPF-RC stimulation during iPSC-derived lung epithelial progenitor cell differentiation. A, Immunofluorescence against SFTPC in day 49 cultures ±IPF-RC. Nuclei stained with DAPI. Scale bars 50 µm. B, $SFTPC^+$ surface area quantified by immunofluorescence. Mean $SFTPC^+$ area per image ±SD. N = 3 independent differentiation rounds. (n = 3 biological replicates per differentiation round and nine images per replicate). $^*P < .05$ by Mann-Whitney U-test. C, H&E and Alcian Blue/PAS stain of iPSC-derived culture cross-sections. Scale bars 50 µm. D, Immunofluorescence against MUC5B in day 49 cultures ±IPF-RC. Nuclei stained with DAPI. Scale bars 40 µm

regions of IPF lungs were lined by MUC5B expressing columnar epithelial cells and displayed extensive mucus plugging. Immunofluorescence further confirmed the presence of $SFTPC^+$ cells in distal IPF patients' lungs, with some cystic lesions lined exclusively by a simple $SFTPC^+$ epithelial cell layer, indicative of ATII cell hyperplasia (Figure 7). The luminal space of some lesions contained yellow appearing material, indicative of a mixture of mucus and surfactant secretions. Interestingly, we also detected cystic lesions that were lined by a metaplastic epithelium characterized by an atypical transition from a $SFTPC^+$ epithelium to a $MUC5B^+$ epithelium in all analyzed IPF samples (Figure 7). These transition zones of ATII-like cells residing in close proximity to goblet-like cells are indicative of a loss of regional epithelial specification and could represent areas of progressing alveolar bronchiolization.

4 | DISCUSSION

In this study, we establish a novel iPSC-derived ALI model of alveolar epithelial differentiation to investigate epithelial dysfunction related to IPF. Utilizing this system, we demonstrate how an IPF-relevant cytokine environment can skew iPSC-derived ATII-like differentiation toward proximal lineages and induce disease-related changes, including secretion of IPF biomarkers. This report thereby describes, for the first time, a human model system that recapitulates key aspects of IPF-related bronchiolization in vitro.

While ALI culture has been applied to human pluripotent stem cell (hPSC)-derived airway epithelial cells to enhance maturation, this method has not yet been tested in hPSC-derived models of the alveolar epithelium.[55,56] We show for the first time, the maturation of hPSC-derived lung epithelial progenitor cells toward ATII-like cells in an ALI culture format, providing a novel platform for both basic research and drug discovery purposes. Our data show that iPSC-derived lung epithelial progenitor cells differentiated at ALI express higher levels of *SFTPC*, *SFTPB*, and *ABCA3* compared to submerged controls. Importantly, $SFTPC^+$ cells are located on the apical surface of the airlifted cultures, suggestive of a positive influence of air exposure on ATII-like differentiation. Interestingly, ABCA3 positive cells, which are not detectable in human fetal lungs prior to 22-23 weeks of gestation, are present within our system.[57] The cultures also express *TM4SF1* which has been described as a marker for alveolar

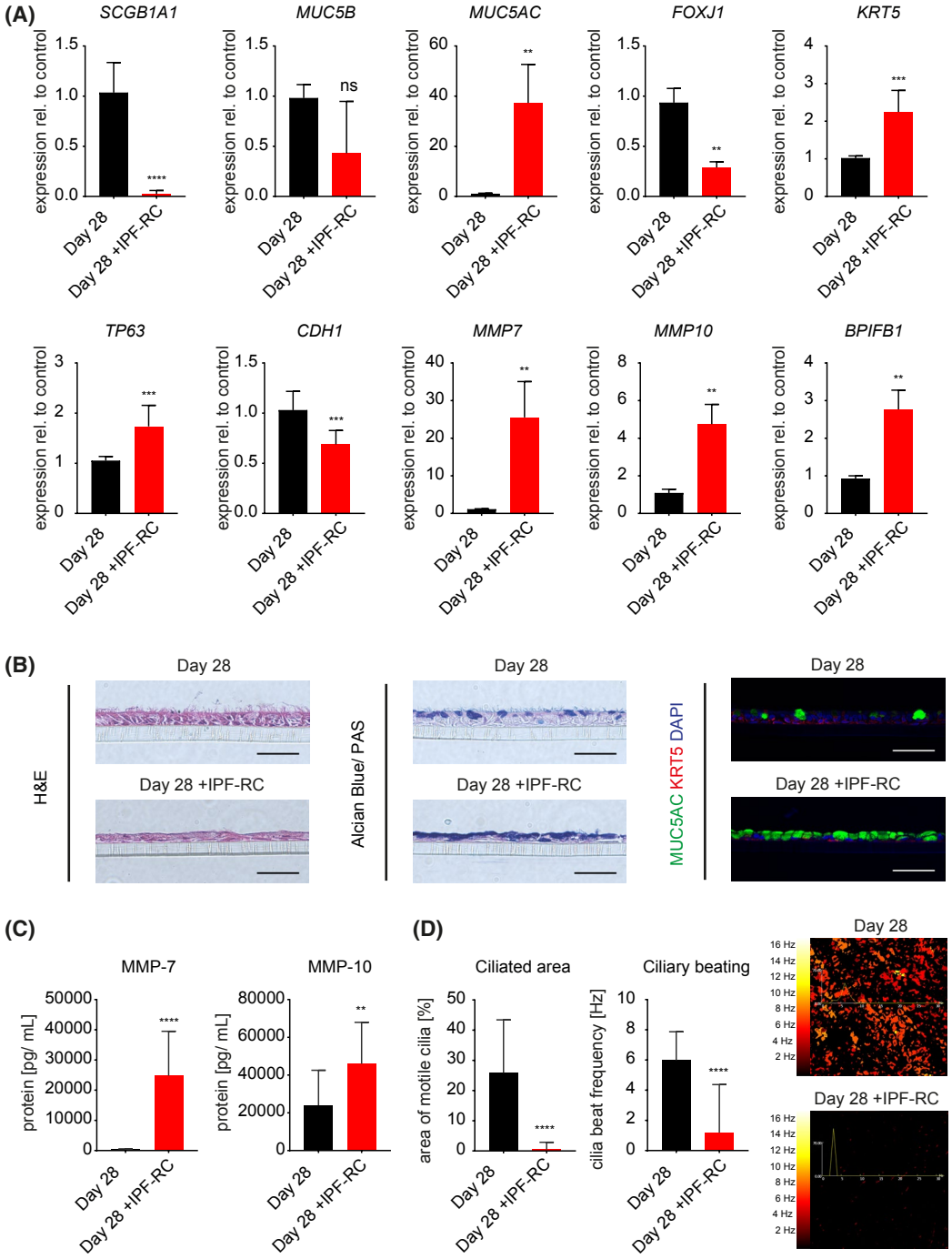

FIGURE 6 IPF-RC-induced alterations in primary human small airway epithelial cell (SAEC) differentiation. A, Gene expression in primary human SAEC cultures normalized to GAPDH relative to untreated controls. Day 28 = SAECs differentiated for 28 days at air-liquid interface culture. Day 28 +IPF-RC = SAECs differentiated for 28 days at air-liquid interface in the presence of IPF-RC. Mean fold change ±SD. N = 3. ns not significant, $^{**}P < .01$, $^{***}P < .001$, and $^{****}P < .0001$ by Mann-Whitney U-test. B, Representative H&E (left), Alcian Blue/PAS stain (middle), and immunofluorescence double stain (right) of primary human SAEC cultures. Immunofluorescence against MUC5AC (green) and KRT5 (red). Nuclei stained with DAPI (blue). Scale bars 50 µm. C, MMP-7 and MMP-10 protein levels in cell culture supernatant of SAEC cultures. Mean ± SD. N = 3. $^{**}P < .01$, and $^{****}P < .0001$ by Mann-Whitney U-test. D, Ciliary beat measurement in SAEC cultures. Mean area covered by motile cilia and mean ciliary beat frequency calculated from N = 3 independent experiments. About 6 regions per insert from 3 biological replicates analyzed per experiment. Error bars represent SD. $^{****}P < .0001$ by Mann-Whitney U-test. Representative regions analyzed for cilia beat measurement shown on the right

epithelial progenitor cells within the adult human lung.[16] In addition, lamellar bodies, ATII specific surfactant producing/storing organelles, are present in the cultures.[28,58-60] Taken together, these results confirm the feasibility of ATII-like cell derivation from iPSC-derived lung progenitor cells in ALI culture.

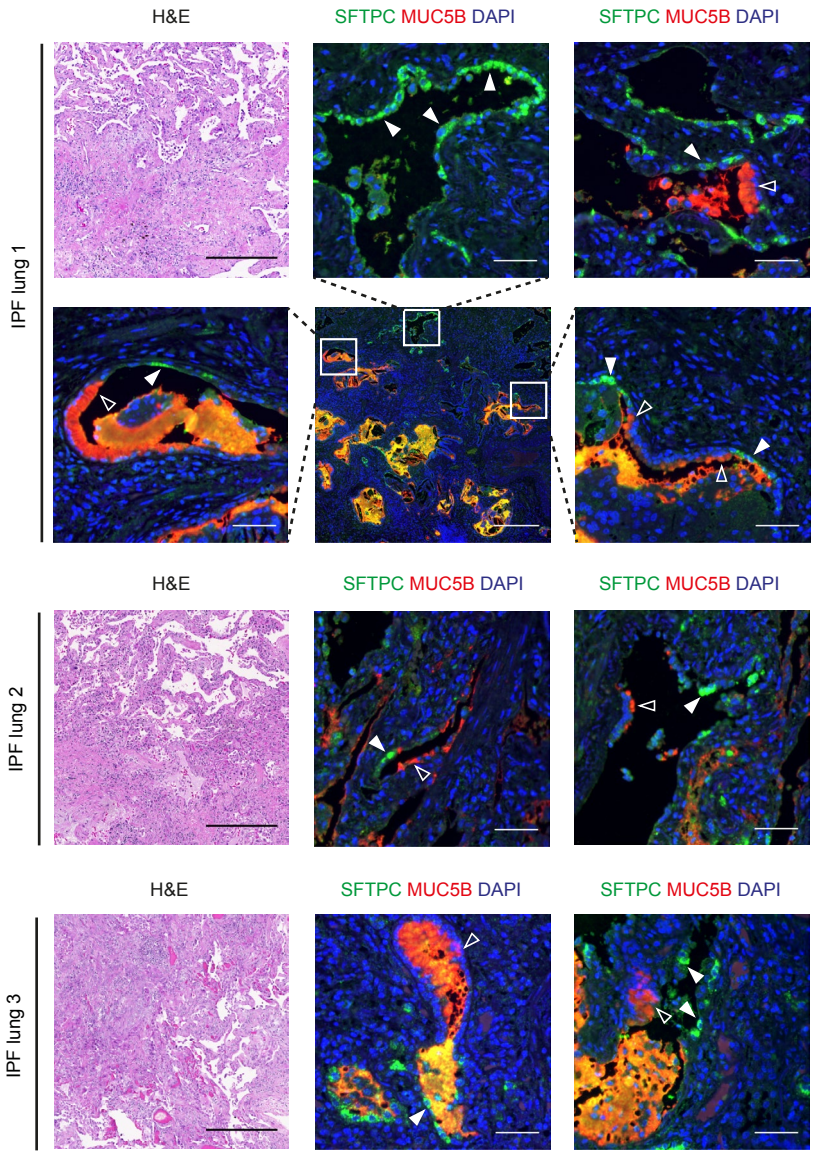

FIGURE 7 Epithelial transition zones in cystic lesions of IPF patient lungs. Representative hematoxylin and eosin stain (H&E) and immunofluorescence against SFTPC (green) and MUC5B (red) in N = 3 human IPF lungs. Epithelial transition zones in cystic lesions lined by $SFTPC^+$ cells (filled arrow heads) and $MUC5B^+$ cells (unfilled arrow heads). Nuclei stained with DAPI (blue). Scale bars 350 μm in H&E images; 50 μm in immunofluorescence images

The disease-specific milieu within the lung has been suggested to play a central role in the pathogenesis of IPF.[61,62] While there is substantial evidence for the relevance of various cytokines and growth factors in IPF, including TGF-β, TGF-α, IL-13, TNF-α and IL-1β, the overexpression of which induces pulmonary fibrosis in animal models, no single factor is known to simultaneously activate all IPF-related pathways.[63,64] Despite this fact, many currently available in vitro models of pulmonary fibrosis rely on a single stimulus.[65] To mimic a pro-fibrotic milieu in vitro, we designed a novel cocktail (IPF-RC) containing nine IPF-relevant cytokines and assessed its effect on differentiating iPSC-derived distal lung epithelial progenitor cells.[35-43] As we primarily aimed to investigate the effect of a fibrosis-relevant environment on progenitors of the alveolar epithelium, IPF-RC stimulation was initiated by day 35 of the protocol, following induction of *SFTPC* expression, which constitutes a specific feature of alveolar epithelial progenitors in fetal human lungs.[66-68]

Analysis of the culture medium in IPF-RC treated cells showed increased MMP-7 and MMP-10, both of which are elevated in IPF patient BAL and serum, and RNA-seq analysis revealed an enrichment of transcripts involved in extracellular matrix organization, indicating an induction of IPF-relevant processes.[69-71] Furthermore, a comparison of transcriptional changes in IPF-RC treated iPSC-derived cultures and human IPF patient lungs revealed a significant overlap of upregulated and downregulated transcripts.[50] On the content, there is also a substantial amount of nonoverlapping deregulated genes, likely both due to the heterogeneity of our culture system and the origin of the publicly available IPF patient data set. The analysis of whole human lung homogenates contains multiple cell types (eg, mesenchymal, endothelial, and immune cells) that are not represented in our in vitro model system. This is supported by the presence of known epithelial-specific transcripts among the commonly deregulated genes, many of which have been associated with lung

fibrosis. In accordance with previous reports, *KLF4*, *VEGFA*, *IL32,* and *SLC19A3* are among the commonly downregulated transcripts.[7,72-74] *BPIFB1* which was described to localize to the bronchiolized epithelium in the honeycomb cysts in usual interstitial pneumonia and *MMP10*, are among the commonly upregulated transcripts.[75,76] Taken together, our iPSC-derived in vitro model mimics certain IPF-related changes in epithelial transcription and secretory phenotype.

In addition, RNA-seq data reveal many known airway associated transcripts with known roles in the developing and adult proximal lung, were among the top upregulated transcripts in IPF-RC treated iPSC-derived cultures, for example, *SOX2*, *PAX9*, *TP63*, *KRT5*, *FOXJ1*, *SCGB1A1,* and *MUC5B*, which have recently been confirmed as markers for the altered IPF lung epithelium via single-cell sequencing.[5,7,9,76-78] Upregulation of airway marker expression following IPF-RC stimulation is accompanied by a loss of ATII specific *SFTPC* expression and a shift in the expression of *SOX2* and *SOX9*, two transcription factors known as central players in proximo-distal epithelial patterning during human and mouse lung development.[28,67] Mouse studies have revealed an essential role of Sox9 during branching morphogenesis, correct distal lung epithelial differentiation during development, as well as recovery of lung function after acute lung injury in adult mice.[79,80] Expression of SOX2, which is associated with proximal airway rather than alveolar identity in healthy lungs, has been shown in the bronchiolized and enlarged distal airspaces in IPF.[5] Moreover, two murine studies have independently shown that selective overexpression of *Sox2* in adult ATII cells resulted in an induction of conducting airway related transcript expression in the alveoli.[81,82] In our study, SOX2 was identified as a putative regulator of the transcriptomic signature associated with IPF-RC treatment by ChIP enrichment analysis (ChEA). Based on previous observations described in the literature and the findings from this study, we hypothesize that SOX2 activation in IPF could promote the bronchiolization-like effect induced by a fibrosis-related cytokine milieu.

Immunohistological analysis of iPSC-derived cultures differentiated in the presence of IPF-RC revealed a significant reduction in $SFTPC^+$ cell area and the emergence $MUC5B^+$ secretory-like cells, an important role of which has been suggested in IPF. Not only has it been shown that $MUC5B^+$ cells abundantly reside within the bronchiolized IPF epithelium, but also a *MUC5B* promoter polymorphism, known to enhance MUC5B expression in the bronchiolo-alveolar epithelia, constitutes the strongest currently known genetic risk factor for IPF.[5,6,83,84] We further demonstrated in this study, that highly aberrant direct transition zones between $SFTPC^+$ and $MUC5B^+$ epithelium exist within distal IPF patient lungs. Based on our findings in a human iPSC-derived alveolar epithelial model and IPF patient lungs, we hypothesize that alveolar epithelial progenitor cells could contribute to epithelial bronchiolization of the distal compartments of the IPF lung via aberrant trans-differentiation toward airway-like lineages.

In our model system, removal of IL-13, but not of any other individual cytokine, from IPF-RC impairs its ability to promote differentiation toward airway-like cell fates at the cost of ATII-like cell differentiation, indicating IL-13 as one of the main drivers of the proximalization effect we observed following IPF-RC stimulation. IL-13 has been described as a main mediator in respiratory diseases, particularly in asthma, where it is linked to mucus secretion and fibrogenic processes.[85] Moreover, IL-13 overexpression leads to pulmonary fibrosis in mice and it has been hypothesized that IL-13 antagonism could constitute a potential treatment strategy for IPF.[86] While IL-13 alone is sufficient to repress *SFTPC* expression, in line with the previous findings in primary human ATII cells,[87] it fails to fully recapitulate the influence of the IPF-RC on airway-specific and IPF-relevant transcripts. Our results are in accordance with the current consensus that neither IL-13, nor any other single factor is sufficient to simultaneously activate all IPF-related pathways in vitro and highlight the importance of more physiological human in vitro model systems.[64] This is underlined by the recent failure of the phase 2 clinical study of tralokinumab, a human anti-IL-13 monoclonal antibody, in subjects with IPF.[88]

It has been proposed that migrating airway stem cells, rather than resident alveolar stem cells, are the stem cell source of the bronchiolized epithelium. As our model system contains rare individual $KRT5^+$ basal-like cells, their role in the IPF-RC mediated effects cannot be excluded. However, as IPF-RC treatment of small airway basal cells induced a strong upregulation of *MUC5AC*, but not *MUC5B*, contrary to the abundant emergence of aberrant $MUC5B^+$ cells in the bronchiolized distal airspaces in IPF patients, as well as suppressed the expression of transcripts upregulated in the IPF lung such as SCGB1A1 and FOXJ1, the airway-like phenotype observed in iPSC-derived IPF-RC cultures is unlikely the sole result of basal-like cell expansion and differentiation.[5,6,76,77] Moreover, IPF-RC stimulation did not induce proliferation of primary small airway basal cells compared to controls. In the future, lineage tracing of $SFTPC^+$ ATII-like cells and $KRT5^+$ basal-like cells should be performed in order to conclusively determine the definite origin of the bronchial-like cells in our iPSC-derived model system.

The usual interstitial pneumonia pattern in IPF is characterized by high temporal and spatial heterogeneity.[89] We hypothesize that our in vitro system utilizing an IPF-relevant cytokine cocktail, could potentially model the progression of epithelial dysfunction from severely affected toward healthy neighboring regions of the lung via a distribution of the pro-fibrotic milieu produced in diseased fibrotic areas within the lung and exposure of epithelial progenitor cells in previously unaffected regions to this milieu. However, as the definite composition of

the IPF BAL/lung milieu is not known, the combination of nine cytokines cannot fully mimic the environment epithelial cells are exposed to in a diseased lung. Moreover, the model utilized in this study does not encapsulate the complex cellular interplay that leads to the vicious cycle of wound repair and scar formation that occurs in IPF,[90] nor the role of genetic risk factors in IPF pathogenesis.[18] In the future, one could envision utilizing this model in coculture with other structural (fibroblasts, endothelial cells) and immune cells, or on the background of preexisting epithelial damage (eg, mechanical wounding) to better understand the role of a pro-fibrotic extracellular milieu in a more physiologically relevant setting.

Overall, our findings highlight that the fibrosis-related milieu present in the IPF lung has the potential to skew alveolar epithelial differentiation toward airway cell phenotypes. Our data suggest that aberrant trans-differentiation of epithelial stem cells in the fibrotic lung could disrupt the regular proximo-distal patterning of the lung epithelium and thereby contribute to the emergence of aberrant epithelial cell types, as well as the apparent bronchiolization in the distal IPF lung. This raises the need for further investigations to determine the exact pathophysiological mechanisms underlying alveolar epithelial cell dysfunction in IPF, which may open routes to novel therapeutic concepts not yet covered by current standard of care therapies.

ACKNOWLEDGMENTS

The research was funded by Boehringer Ingelheim Pharma GmbH & Co. KG. JPG was also supported by a UK Medical Research Foundation Fellowship (MRF-091-0001-RG-GARNE).

CONFLICT OF INTEREST

ES, VS, HQL, TS, DR, ELS, KFC, TB, SW, MS, MJT, RH, MJW, MD, BS, KQ, and JPG are employees of Boehringer Ingelheim Pharma GmbH & Co. KG.

AUTHOR CONTRIBUTIONS

J.P. Garnett, E. Schruf, and R. Heilker designed research; E. Schruf, V. Schroeder, T. Schönberger, D. Raedel, E.L. Stewart, S. Weigle, M.J. Webster, and T. Bluhmki performed research; E. Schruf, V. Schroeder, K. Quast, K. Fundel-Clemens, H.Q. Le, D. Raedel, M. Schuler, S. Weigle, M.J. Webster, and B. Stierstorfer analyzed data; K. Quast supervised the bioinformatics analysis; M. Dass oversaw the electron microscopy analysis; B. Stierstorfer reviewed and provided IPF lung samples; E. Schruf, J.P. Garnett, H.Q. Le, K. Quast, B. Stierstorfer, M. Frick, M. Schuler, M. Dass, and M.J. Thomas wrote the paper.

DATA AVAILABILITY STATEMENT

The data sets generated during and/or analyzed during the current study are available from the corresponding author on reasonable request.

REFERENCES

1. Raghu G, Collard HR, Egan JJ, et al. An official ATS/ERS/JRS/ALAT statement: idiopathic pulmonary fibrosis: evidence-based guidelines for diagnosis and management. *Am J Respir Crit Care Med*. 2011;183:788-824.
2. Lederer DJ, Martinez FJ. Idiopathic pulmonary fibrosis. *N Engl J Med*. 2018;378:1811-1823.
3. Ryu JH, Moua T, Daniels CE, et al. Idiopathic pulmonary fibrosis: evolving concepts. *Mayo Clin Proc*. 2014;89:1130-1142.
4. Chambers RC, Mercer PF. Mechanisms of alveolar epithelial injury, repair, and fibrosis. *Ann Am Thorac Soc*. 2015;12(Suppl 1):S16-S20.
5. Plantier L, Crestani B, Wert SE, et al. Ectopic respiratory epithelial cell differentiation in bronchiolised distal airspaces in idiopathic pulmonary fibrosis. *Thorax*. 2011;66:651-657.
6. Seibold MA, Smith RW, Urbanek C, et al. The idiopathic pulmonary fibrosis honeycomb cyst contains a mucocilary pseudostratified epithelium. *PLoS ONE*. 2013;8:e58658.
7. Xu Y, Mizuno T, Sridharan A, et al. Single-cell RNA sequencing identifies diverse roles of epithelial cells in idiopathic pulmonary fibrosis. *JCI Insight*. 2016;1:e90558.
8. Kim CF, Jackson EL, Woolfenden AE, et al. Identification of bronchioalveolar stem cells in normal lung and lung cancer. *Cell*. 2005;121:823-835.
9. Smirnova NF, Schamberger AC, Nayakanti S, Hatz R, Behr J, Eickelberg O. Detection and quantification of epithelial progenitor cell populations in human healthy and IPF lungs. *Respir Res*. 2016;17:83.
10. Akram KM, Lomas NJ, Spiteri MA, Forsyth NR. Club cells inhibit alveolar epithelial wound repair via TRAIL-dependent apoptosis. *Eur Respir J*. 2013;41:683-694.
11. Kumar PA, Hu Y, Yamamoto Y, et al. Distal airway stem cells yield alveoli in vitro and during lung regeneration following H1N1 influenza infection. *Cell*. 2011;147:525-538.
12. Rawlins EL, Okubo T, Xue Y, et al. The role of Scgb1a1+ Clara cells in the long-term maintenance and repair of lung airway, but not alveolar, epithelium. *Cell Stem Cell*. 2009;4:525-534.
13. Zepp JA, Zacharias WJ, Frank DB, et al. Distinct mesenchymal lineages and niches promote epithelial self-renewal and myofibrogenesis in the lung. *Cell*. 2017;170:1134-1148.e10.
14. Nabhan AN, Brownfield DG, Harbury PB, Krasnow MA, Desai TJ. Single-cell Wnt signaling niches maintain stemness of alveolar type 2 cells. *Science*. 2018;359:1118-1123.
15. Barkauskas CE, Cronce MJ, Rackley CR, et al. Type 2 alveolar cells are stem cells in adult lung. *J Clin Invest*. 2013;123:3025-3036.
16. Zacharias WJ, Frank DB, Zepp JA, et al. Regeneration of the lung alveolus by an evolutionarily conserved epithelial progenitor. *Nature*. 2018;555:251-255.
17. Knudsen L, Ruppert C, Ochs M. Tissue remodelling in pulmonary fibrosis. *Cell Tissue Res*. 2017;367:607-626.
18. Winters NI, Burman A, Kropski JA, Blackwell TS. Epithelial injury and dysfunction in the pathogenesis of idiopathic pulmonary fibrosis. *Am J Med Sci*. 2019;357:374-378.
19. Mao P, Wu S, Li J, et al. Human alveolar epithelial type II cells in primary culture. *Physiol Rep*. 2015;3:e12288.
20. Huang SX, Islam MN, O'Neill J, et al. Efficient generation of lung and airway epithelial cells from human pluripotent stem cells. *Nat Biotechnol*. 2014;32:84-91.

21. Gotoh S, Ito I, Nagasaki T, et al. Generation of alveolar epithelial spheroids via isolated progenitor cells from human pluripotent stem cells. *Stem Cell Reports*. 2014;3:394-403.
22. Chen Y, Feng J, Zhao S, et al. Long-term engraftment promotes differentiation of alveolar epithelial cells from human embryonic stem cell derived lung organoids. *Stem Cells Dev*. 2018;27:1339-1349.
23. Jacob A, Morley M, Hawkins F, et al. Differentiation of human pluripotent stem cells into functional lung alveolar epithelial cells. *Cell Stem Cell*. 2017;21:472-488.e10.
24. Yamamoto Y, Gotoh S, Korogi Y, et al. Long-term expansion of alveolar stem cells derived from human iPS cells in organoids. *Nat Methods*. 2017;14:1097-1106.
25. de Carvalho A, Strikoudis A, Liu HY, et al. Glycogen synthase kinase 3 induces multilineage maturation of human pluripotent stem cell-derived lung progenitors in 3D culture. *Development*. 2019;146:dev171652.
26. Miller AJ, Hill DR, Nagy MS, et al. In vitro induction and in vivo engraftment of lung bud tip progenitor cells derived from human pluripotent stem cells. *Stem Cell Reports*. 2018;10:101-119.
27. Chen YW, Huang SX, de Carvalho A, et al. A three-dimensional model of human lung development and disease from pluripotent stem cells. *Nat Cell Biol*. 2017;19:542-549.
28. Nikolic MZ, Sun D, Rawlins EL. Human lung development: recent progress and new challenges. *Development*. 2018;145:dev163485.
29. Whitsett JA, Haitchi HM, Maeda Y. Intersections between pulmonary development and disease. *Am J Respir Crit Care Med*. 2011;184:401-406.
30. Bertoncello I. Properties of adult lung stem and progenitor cells. *J Cell Physiol*. 2016;231:2582-2589.
31. Kotton DN, Morrisey EE. Lung regeneration: mechanisms, applications and emerging stem cell populations. *Nat Med*. 2014;20:822-832.
32. Shi W, Xu J, Warburton D. Development, repair and fibrosis: what is common and why it matters. *Respirology*. 2009;14:656-665.
33. Sakai N, Tager AM. Fibrosis of two: epithelial cell-fibroblast interactions in pulmonary fibrosis. *Biochem Biophys Acta*. 2013;1832:911-921.
34. Selman M, Pardo A, Kaminski N. Idiopathic pulmonary fibrosis: aberrant recapitulation of developmental programs? *PLoS Med*. 2008;5:e62.
35. Tasaka S, Mizoguchi K, Funatsu Y, et al. Cytokine profile of bronchoalveolar lavage fluid in patients with combined pulmonary fibrosis and emphysema. *Respirology*. 2012;17:814-820.
36. Zhang Y, Bi L, Qiu Y, et al. Elevated sL1-CAM levels in BALF and serum of IPF patients. *Respirology*. 2016;21:143-148.
37. Bellanger AP, Gbaguidi-Haore H, Gondoin A, et al. Positive fungal quantitative PCR and Th17 cytokine detection in bronchoalveolar lavage fluids: complementary biomarkers of hypersensitivity pneumonitis? *J Immunol Methods*. 2016;434:61-65.
38. Meloni F, Caporali R, Marone Bianco A, et al. BAL cytokine profile in different interstitial lung diseases: a focus on systemic sclerosis. *Sarcoidosis Vasc Diffuse Lung Dis*. 2004;21:111-118.
39. Vasakova M, Sterclova M, Kolesar L, et al. Bronchoalveolar lavage fluid cellular characteristics, functional parameters and cytokine and chemokine levels in interstitial lung diseases. *Scand J Immunol*. 2009;69:268-274.
40. Barlo NP, van Moorsel CH, Korthagen NM, et al. Genetic variability in the IL1RN gene and the balance between interleukin (IL)-1 receptor agonist and IL-1beta in idiopathic pulmonary fibrosis. *Clin Exp Immunol*. 2011;166:346-351.
41. Guiot J, Henket M, Corhay JL, Moermans C, Louis R. Sputum biomarkers in IPF: evidence for raised gene expression and protein level of IGFBP-2, IL-8 and MMP-7. *PLoS ONE*. 2017;12:e0171344.
42. Lee JU, Chang HS, Lee HJ, et al. Upregulation of interleukin-33 and thymic stromal lymphopoietin levels in the lungs of idiopathic pulmonary fibrosis. *BMC pulmonary medicine*. 2017;17:39.
43. Park SW, Ahn MH, Jang HK, et al. Interleukin-13 and its receptors in idiopathic interstitial pneumonia: clinical implications for lung function. *J Korean Med Sci*. 2009;24:614-620.
44. Huang SX, Green MD, de Carvalho AT, et al. The in vitro generation of lung and airway progenitor cells from human pluripotent stem cells. *Nat Protoc*. 2015;10:413-425.
45. Sollner JF, Leparc G, Hildebrandt T, et al. An RNA-Seq atlas of gene expression in mouse and rat normal tissues. *Sci Data*. 2017;4:170185.
46. Ritchie ME, Phipson B, Wu D, et al. limma powers differential expression analyses for RNA-sequencing and microarray studies. *Nucleic Acids Res*. 2015;43:e47.
47. Metsalu T, Vilo J. ClustVis: a web tool for visualizing clustering of multivariate data using Principal Component Analysis and heatmap. *Nucleic Acids Res*. 2015;43:W566-W570.
48. Subramanian A, Tamayo P, Mootha VK, et al. Gene set enrichment analysis: a knowledge-based approach for interpreting genome-wide expression profiles. *Proc Natl Acad Sci U S A*. 2005;102:15545-15550.
49. Liberzon A, Birger C, Thorvaldsdottir H, Ghandi M, Mesirov JP, Tamayo P. The Molecular Signatures Database (MSigDB) hallmark gene set collection. *Cell Syst*. 2015;1:417-425.
50. Kusko RL, Brothers JF 2nd, Tedrow J, et al. Integrated genomics reveals convergent transcriptomic networks underlying chronic obstructive pulmonary disease and idiopathic pulmonary fibrosis. *Am J Respir Crit Care Med*. 2016;194:948-960.
51. Keenan AB, Torre D, Lachmann A, et al. ChEA3: transcription factor enrichment analysis by orthogonal omics integration. *Nucleic Acids Res*. 2019;47:W212-W224.
52. Schindelin J, Arganda-Carreras I, Frise E, et al. Fiji: an open-source platform for biological-image analysis. *Nat Methods*. 2012;9:676-682.
53. Weigle S, Martin E, Voegtle A, Wahl B, Schuler M. Primary cell-based phenotypic assays to pharmacologically and genetically study fibrotic diseases in vitro. *J Biol Methods*. 2019;6(2):115.
54. Schruf E, Schroeder V, Kuttruff CA, et al. Human lung fibroblast-to-myofibroblast transformation is not driven by an LDH5-dependent metabolic shift towards aerobic glycolysis. *Respir Res*. 2019;20:87.
55. Wong AP, Bear CE, Chin S, et al. Directed differentiation of human pluripotent stem cells into mature airway epithelia expressing functional CFTR protein. *Nat Biotechnol*. 2012;30:876-882.
56. Firth AL, Dargitz CT, Qualls SJ, et al. Generation of multiciliated cells in functional airway epithelia from human induced pluripotent stem cells. *Proc Natl Acad Sci U S A*. 2014;111:E1723-E1730.
57. Stahlman MT, Besnard V, Wert SE, et al. Expression of ABCA3 in developing lung and other tissues. *J Histochem Cytochem*. 2007;55:71-83.
58. Van der Velden JL, Bertoncello I, McQualter JL. LysoTracker is a marker of differentiated alveolar type II cells. *Respir Res*. 2013;14:123.

59. Chander A, Johnson RG, Reicherter J, Fisher AB. Lung lamellar bodies maintain an acidic internal pH. *J Biol Chem*. 1986;261:6126-6131.
60. Baritussio AG, Magoon MW, Goerke J, Clements JA. Precursor-product relationship between rabbit type II cell lamellar bodies and alveolar surface-active material. Surfactant turnover time. *Biochem Biophys Acta*. 1981;666:382-393.
61. Agostini C, Gurrieri C. Chemokine/cytokine cocktail in idiopathic pulmonary fibrosis. *Proc Am Thorac Soc*. 2006;3:357-363.
62. Xu X, Dai H, Wang C. Epithelium-dependent profibrotic milieu in the pathogenesis of idiopathic pulmonary fibrosis: current status and future directions. *Clin Respir J*. 2016;10:133-141.
63. B. Moore B, Lawson WE, Oury TD, Sisson TH, Raghavendran K, Hogaboam CM. Animal models of fibrotic lung disease. *Am J Respir Cell Mol Biol*. 2013;49:167-179.
64. King TE, Pardo A, Selman M. Idiopathic pulmonary fibrosis. *Lancet*. 2011;378:1949-1961.
65. Sundarakrishnan A, Chen Y, Black LD, Aldridge BB, Kaplan DL. Engineered cell and tissue models of pulmonary fibrosis. *Adv Drug Deliv Rev*. 2018;129:78-94.
66. Khoor A, Stahlman MT, Gray ME, Whitsett JA. Temporal-spatial distribution of SP-B and SP-C proteins and mRNAs in developing respiratory epithelium of human lung. *J Histochem Cytochem*. 1994;42:1187-1199.
67. Nikolic MZ, Caritg O, Jeng Q, et al. Human embryonic lung epithelial tips are multipotent progenitors that can be expanded in vitro as long-term self-renewing organoids. *Elife*. 2017;6:e26575.
68. Treutlein B, Brownfield DG, Wu AR, et al. Reconstructing lineage hierarchies of the distal lung epithelium using single-cell RNA-seq. *Nature*. 2014;509:371-375.
69. Rosas IO, Richards TJ, Konishi K, et al. MMP1 and MMP7 as potential peripheral blood biomarkers in idiopathic pulmonary fibrosis. *PLoS Med*. 2008;5:e93.
70. Maher TM, Oballa E, Simpson JK, et al. An epithelial biomarker signature for idiopathic pulmonary fibrosis: an analysis from the multicentre PROFILE cohort study. *Lancet Respir Med*. 2017;5:946-955.
71. Sokai A, Handa T, Tanizawa K, et al. Matrix metalloproteinase-10: a novel biomarker for idiopathic pulmonary fibrosis. *Respir Res*. 2015;16:120.
72. Lin L, Han Q, Xiong Y, et al. Krupple-like-factor 4 attenuates lung fibrosis via inhibiting epithelial-mesenchymal transition. *Sci Rep*. 2017;7:15847.
73. Murray LA, Habiel DM, Hohmann M, et al. Antifibrotic role of vascular endothelial growth factor in pulmonary fibrosis. *JCI Insight*. 2017;2:e92192.
74. Hong GH, Park SY, Kwon HS, et al. IL-32gamma attenuates airway fibrosis by modulating the integrin-FAK signaling pathway in fibroblasts. *Respir Res*. 2018;19:188.
75. Bingle CD, Araujo B, Wallace WA, Hirani N, Bingle L. What is top of the charts? BPIFB1/LPLUNC1 localises to the bronchiolised epithelium in the honeycomb cysts in UIP. *Thorax*. 2013;68:1167-1168.
76. Yang IV, Coldren CD, Leach SM, et al. Expression of cilium-associated genes defines novel molecular subtypes of idiopathic pulmonary fibrosis. *Thorax*. 2013;68:1114-1121.
77. Buendia-Roldan I, Ruiz V, Sierra P, et al. Increased expression of CC16 in patients with idiopathic pulmonary fibrosis. *PLoS ONE*. 2016;11:e0168552.
78. McDonough JE, Kaminski N, Thienpont B, Hogg JC, Vanaudenaerde BM, Wuyts WA. Gene correlation network analysis to identify regulatory factors in idiopathic pulmonary fibrosis. *Thorax*. 2019;74:132-140.
79. Rockich BE, Hrycaj SM, Shih HP, et al. Sox9 plays multiple roles in the lung epithelium during branching morphogenesis. *Proc Natl Acad Sci U S A*. 2013;110:E4456-E4464.
80. Li L, Zhang H, Min D, et al. Sox9 activation is essential for the recovery of lung function after acute lung injury. *Cell Physiol Biochem*. 2015;37:1113-1122.
81. Tompkins DH, Besnard V, Lange AW, et al. Sox2 activates cell proliferation and differentiation in the respiratory epithelium. *Am J Respir Cell Mol Biol*. 2011;45:101-110.
82. Kapere Ochieng J, Schilders K, Kool H, et al. Differentiated type II pneumocytes can be reprogrammed by ectopic Sox2 expression. *PLoS ONE*. 2014;9:e107248.
83. Seibold MA, Wise AL, Speer MC, et al. A common MUC5B promoter polymorphism and pulmonary fibrosis. *N Engl J Med*. 2011;364:1503-1512.
84. Evans CM, Fingerlin TE, Schwarz MI, et al. Idiopathic pulmonary fibrosis: a genetic disease that involves mucociliary dysfunction of the peripheral airways. *Physiol Rev*. 2016;96:1567-1591.
85. Passalacqua G, Mincarini M, Colombo D, et al. IL-13 and idiopathic pulmonary fibrosis: possible links and new therapeutic strategies. *Pulm Pharmacol Ther*. 2017;45:95-100.
86. Lee CG, Homer RJ, Zhu Z, et al. Interleukin-13 induces tissue fibrosis by selectively stimulating and activating transforming growth factor beta(1). *J Exp Med*. 2001;194:809-821.
87. Seibold MA. Interleukin-13 stimulation reveals the cellular and functional plasticity of the airway epithelium. *Ann Am Thorac Soc*. 2018;15:S98-S102.
88. Parker JM, Glaspole IN, Lancaster LH, et al. A phase 2 randomized controlled study of tralokinumab in subjects with idiopathic pulmonary fibrosis. *Am J Respir Crit Care Med*. 2018;197:94-103.
89. Smith M, Dalurzo M, Panse P, Parish J, Leslie K. Usual interstitial pneumonia-pattern fibrosis in surgical lung biopsies. Clinical, radiological and histopathological clues to aetiology. *J Clin Pathol*. 2013;66:896-903.
90. Selman M, Pardo A. Idiopathic pulmonary fibrosis: an epithelial/fibroblastic cross-talk disorder. *Respir Res*. 2002;3:3.

SUPPORTING INFORMATION

Additional supporting information may be found online in the Supporting Information section.

How to cite this article: Schruf E, Schroeder V, Le HQ, et al. Recapitulating idiopathic pulmonary fibrosis related alveolar epithelial dysfunction in a human iPSC-derived air-liquid interface model. *The FASEB Journal*. 2020;00:1–22. https://doi.org/10.1096/fj.201902926R